EBioMedicine 61 (2020) 103034

Contents lists available at ScienceDirect

EBioMedicine

journal homepage: www.elsevier.com/locate/ebiom

Research paper

Canonical WNT pathway is activated in the airway epithelium in chronic obstructive pulmonary disease

François M. Carlier[a,b], Sébastien Dupasquier[a], Jérôme Ambroise[c], Bruno Detry[a], Marylène Lecocq[a], Charline Biétry–Claudet[a], Yassine Boukala[a], Jean-Luc Gala[c], Caroline Bouzin[d], Stijn E. Verleden[e], Delphine Hoton[f], Sophie Gohy[a,g], Bertrand Bearzatto[c], Charles Pilette[a,g,*]

[a] Pole of Pneumology, ENT, and Dermatology, Institute of Experimental and Clinical Research, Université catholique de Louvain, Brussels, Belgium
[b] Department of Pneumology, CHU Mont-Godinne UCL Namur, Yvoir, Belgium
[c] Centre de Technologies Moléculaires Appliquées, Institute of Experimental and Clinical Research, Université catholique de Louvain, Brussels, Belgium
[d] IREC Imaging Platform, Institute of Experimental and Clinical Research, Université catholique de Louvain, Brussels, Belgium
[e] Lung Transplant Unit, Division of Respiratory Disease, Department of Clinical and Experimental Medicine, Katholieke Universiteit Leuven, Leuven, Belgium
[f] Department of Clinical Laboratory, Cliniques Universitaires Saint-Luc, Brussels, Belgium
[g] Department of Pneumology, Cliniques Universitaires Saint-Luc, Brussels, Belgium

ARTICLE INFO

Article History:
Received 3 April 2020
Revised 10 September 2020
Accepted 14 September 2020
Available online 10 October 2020

Keywords:
COPD
WNT
β-catenin
Airway epithelium
Barrier dysfunction

ABSTRACT

Background: Chronic obstructive pulmonary disease (COPD) is a devastating lung disease, mainly due to cigarette smoking, which represents the third cause of mortality worldwide. The mechanisms driving its epithelial salient features remain largely elusive. We aimed to evaluate the activation and the role of the canonical, β-catenin-dependant WNT pathway in the airway epithelium from COPD patients.
Methods: The WNT/β-catenin pathway was first assessed by WNT-targeted RNA sequencing of the air/liquid interface-reconstituted bronchial epithelium from COPD and control patients. Airway expression of total and active β-catenin was assessed in lung sections, as well as WNT components in laser-microdissected airway epithelium. Finally, we evaluated the role of WNT at the bronchial epithelial level by modulating the pathway in the reconstituted COPD epithelium.
Findings: We show that the WNT/β-catenin pathway is upregulated in the COPD airway epithelium as compared with that of non-smokers and control smokers, in targeted RNA-sequencing of *in vitro* reconstituted airway epithelium, and *in situ* in lung tissue and laser-microdissected epithelium. Extrinsic activation of this pathway in COPD-derived airway epithelium inhibited epithelial differentiation, polarity and barrier function, and induced TGF-β-related epithelial-to-mesenchymal transition (EMT). Conversely, canonical WNT inhibition increased ciliated cell numbers, epithelial polarity and barrier function, whilst inhibiting EMT, thus reversing COPD features.
Interpretation: In conclusion, the aberrant reactivation of the canonical WNT pathway in the adult airway epithelium recapitulates the diseased phenotype observed in COPD patients, suggesting that this pathway or its downstream effectors could represent a future therapeutic target.
Funding: This study was supported by the Fondation Mont-Godinne, the FNRS and the WELBIO.

1. Introduction

Chronic obstructive pulmonary disease (COPD) is a major health burden and is currently the third leading cause of death worldwide, according to World Health Organization estimations [1]. Its major cause is cigarette smoking, although genetic predisposition and other toxic exposures (air pollution, occupational, biomass) may also play a role [2]. COPD is characterized by a slowly progressive and mostly irreversible airway obstruction that is due to a combination of small airway disease (with mucus plugs and peribronchial fibrosis) and emphysema (destruction of the alveolar walls), ultimately leading to respiratory failure [3]. Besides alveoli and small airways, large airways are also altered in COPD, with inflammation [4], increased

* Corresponding author at: Pole of Pneumology, ENT, and Dermatology, Institute of Experimental and Clinical Research (Université catholique de Louvain), Avenue Mounier, 54 B1.54.04, 1200 Brussels, Belgium
E-mail address: charles.pilette@uclouvain.be (C. Pilette).

https://doi.org/10.1016/j.ebiom.2020.103034

Research in context

Evidence before this study

Chronic obstructive pulmonary disease (COPD) is the third cause of death worldwide. Developmental pathways are thought to play a crucial role in its pathophysiology, including WNT signalling. While the canonical WNT pathway is dysregulated in COPD at the alveolar level, its role in the proximal airway epithelium remains elusive.

Added value of this study

Using *in situ* analysis of surgical airway tissue and *in vitro* cell cultures, we show that the canonical WNT pathway is activated in the adult COPD bronchial epithelium and that this activation recapitulates the COPD phenotype. In contrast, inhibiting the canonical WNT pathway in COPD-derived cultures reversed the epithelial pathology *in vitro*.

Implications of all the available evidence

We provide new evidence that the canonical WNT pathway is a key regulator of the human airway epithelium and could represent a valuable therapeutic target for the treatment of COPD.

extracellular matrix deposition[5], lineage abnormalities[6] and barrier dysfunction of the epithelium [7]. The relevance of large airway disease in COPD relates to its association with increased risk of exacerbations and of lung cancer [8,9].

Discovered in the early 1980s [10], the Wingless/Integrase-1 (WNT) signalling pathways play a crucial role in lung morphogenesis [11] and have been widely studied in chronic respiratory diseases [12,13]. Canonical WNT signalling involves the activation of the transcriptional coactivator β-catenin, while noncanonical WNT signalling is β-catenin independent and subdivided in planar polarity cell signalling, calcium/calmodulin-dependant protein kinase II signalling, and other less well-defined cascades [14]. In the absence of canonical WNT stimulation (*e.g.* WNT-3a and WNT-8), the so-called "β-catenin destruction complex" regulates the pool of intracellular β-catenin by phosphorylation and ubiquitination, ultimately addressing β-catenin to proteasomal degradation [15]. This prevents its migration to the nucleus, where expression of WNT target genes is constitutively repressed by a complex consisting of T-cell factor/lymphoid enhancer-binding factor (TCF/LEF) and transducing-like enhancer of split protein (TLE/Groucho). The binding of a canonical WNT ligand to one of the Frizzled receptors (FZD_{1-10}) leads to the inactivation of the destruction complex and to the accumulation of intracytoplasmic, unphosphorylated β-catenin, whose migration to the nucleus will transactivate its target genes [16], including epithelial-to-mesenchymal (EMT)-promoting transcription factors[17].

WNT pathways have been studied in COPD where persistent reactivation of developmental pathways – such as WNT, Notch, Sonic hedgehog, as well as TGF-β – emerged as a new paradigm [18]. Previous studies showed that upregulated noncanonical WNT signalling, through increased WNT-5a and −5b [19,20], contributes to emphysema (characterized by the disruption of alveolar walls) by negatively regulating alveolar repair, while decreased FZD4 in COPD leads to reduced canonical signalling and impaired alveolar repair capacity [21]. On the other hand, extrinsic activation of the canonical pathway (by LiCl or CHIR99021) in elastase-induced murine emphysema[22] and *ex-vivo* three-dimensional murine lung tissue cultures [23] attenuated those COPD features at the alveolar level. Moreover, the FAM13A gene, associated with COPD in genome-wide association studies [24], is suspected to promote β-catenin degradation, increasing disease susceptibility in murine elastase-induced emphysema [25]. Taken together, these results suggest a shift from canonical to noncanonical WNT signalling in the COPD alveolar epithelium that underlies emphysema.

In contrast, data regarding WNT dysregulation at the *airway* epithelium (AE) level remain controversial. Thus, the noncanonical ligand WNT-4 was upregulated in COPD bronchial biopsies [26], and potentiated cigarette smoke-induced inflammation in 16HBE cells [27]. The expression of noncanonical ligands WNT-4 and −5b was increased in COPD-derived primary human bronchial epithelial cells (HBECs) redifferentiated upon air/liquid interface (ALI), compared with controls [27,28]. Nicotine-exposed HBECs showed increased canonical WNT-3a expression that further induced EMT [29], and the canonical FZD8 receptor was found to promote epithelial inflammation in cigarette smoke-exposed mice [30]. The activation of the WNT/β-catenin pathway by CHIR99021 in ALI-HBEC also inhibited the commitment towards ciliated cells [31]. Conversely it was however shown that several canonical components, including β-catenin, were downregulated in the small AE from COPD patients, either from endobronchial biopsies and brushings [32], or surgical lung tissue [33]. Globally, these results consistently show an activation of the noncanonical WNT pathways in the proximal AE in COPD, while divergent results are seen concerning the WNT/β-catenin pathway.

EMT is a dynamic process where epithelial cells lose their polarity and adhesiveness, and gain migratory abilities and mesenchymal features. EMT programming is crucial to embryogenesis (type I EMT), tissue repair (type II), and cancer metastasis (type III), and is regulated by an intricate network of pathways, including WNT and TGF-β [34]. In the last decade, several studies showed that EMT occurs in the COPD AE, both in small[35] and large airways [36,37], therefore promoting airway fibrosis, impaired epithelial repair, as well as carcinogenesis and metastasis potential [38,39]. It was reported that ALI-cultures from COPD patients spontaneously display mesenchymal features and that cigarette smoke may induce EMT in control HBECs, possibly as a result of TGF-β signalling [40]. Moreover, upon TGF-β_1 stimulation, pulmonary fibroblasts from COPD patients seemed more prone to express EMT features (fibronectin, collagen-1α1, α-smooth muscle actin), in a WNT/β-catenin dependant fashion [41]. Although canonical WNT activation has been extensively reported in (idiopathic) pulmonary fibrosis, as recently rewiewed [12], little is known about the role of WNT in EMT-related COPD airway fibrosis.

In the present study, we aimed at clarifying whether the WNT/β-catenin pathway is activated in the proximal AE in COPD and at addressing the hypothesis that WNT dysregulation contributes to the aberrant airway epithelial phenotype observed in this disease, including EMT.

2. Materials and methods

2.1. Experimental design, study population and lung tissue samples

A series of lung surgical specimens containing large airways was selected from five different patients groups (non-smokers, smoker controls, mild COPD, moderate COPD and severe to very severe COPD). COPD patients were sorted on basis of their pulmonary function tests, according to the GOLD 2001 classification. Patients with any other lung disease than COPD (*e.g.* asthma, pulmonary fibrosis) were excluded from the study. All patients received information and signed a written consent to the study protocol, which was approved by the local clinical Ethical committee (reference 2007/19MARS/58 for UCLouvain, S52174 and S55877 for KULeuven). Smoking history was recorded according to patient reporting, a status of former smoker referring to as patients who quitted smoking at least 12 months before surgery. A primary proximal bronchial epithelium was reconstituted *in vitro* from all subjects as described hereunder, and was subjected to WNT-targeted RNA-sequencing (RNA-seq,

n = 47 subjects), RT-qPCR for validation (n = 21), and WNT modulation experiments (n = 6). In parallel, the surgical specimens were embedded for immunostaining of the bronchial epithelium (n = 56). Patients' characteristics are shown in Tables 1–3, and S1.

2.2. In vitro *reconstitution of primary human bronchial epithelium on Ali culture*

A large piece of cartilaginous bronchus was selected from lobectomies or explants, located as far as possible from the tumour site (in the case of lobectomies) and submitted to pronase digestion overnight at 4 °C, in order to HBECs. HBECs were cultured in flasks in retinoic acid-supplemented Bronchial Epithelial Cell Growth Basal Medium (Lonza, Verviers, Belgium) until confluence. Cells were then detached and seeded at a density of 80,000 cells/well on 24-well polyester filter-type inserts (0•4-μm pore size; Corning, Corning, NY) coated with 0•2 mg/ml collagen IV (Sigma-Aldrich, Saint-Louis, MO) until a confluent monolayer was obtained. The culture was then carried out in air/liquid interface (ALI) for 14 to 21 days, according to the experiment. Once in ALI, HBECs were cultured in BEBM:DMEM (1:1) medium supplemented with penicillin (100 U/ml), streptomycin (100 μg/ml) (Lonza), bovine serum albumin (BSA) (1•5 μg/ml), retinoic acid (30 ng/ml) (Sigma-Aldrich), and BEGM SingleQuots™ Supplements and Growth Factors (Lonza), including bovine pituitary extract (52 μg/ml), insulin (5 μg/ml), hydrocortisone (0•5 g/ml), transferrin (10 μg/ml), adrenaline (0•5 μg/ml), epidermal growth factor (0•5 ng/ml) and triiodothyronine (3•25 ng/ml).

At the end of the ALI culture, basolateral media were collected, and the apical pole of HBEC was washed with 300 μl sterile PBS, then centrifuged for 5 min at 10,000 g. Transwell inserts were fixed by direct immersion in 4% buffered formaldehyde, before incubation in PBS at pH 7•4 and embedding in paraffin blocks. ALI-HBEC were also processed for gene expression or Western blot analyses (see below).

The modulation of the WNT/β-catenin pathway was performed in 6 very severe COPD-derived ALI-HBECs, by adding to the culture medium either the canonical WNT activator CHIR99021 (Sigma-Aldrich; 10 μM) or the canonical WNT inhibitor XAV939 (Sigma-Aldrich; 10 μM) for 5 days at different predefined time-periods: ALI D6-D10 (referred to as T1), D11-D15 (T2) or D16-D20 (T3). The absence of significant toxicity at those concentrations was confirmed by using a LDH release assay.

2.3. Targeted RNA-sequencing

2.3.1. RNA isolation and quantification

RNA was isolated from 70, ALI cultures at 2 weeks, in order to establish signature genes in pure cultures of airway epithelial cells at an early differentiation time-point. RiboPure™ RNA Purification kit

Table 1
Patient series for epithelial WNT-targeted RNA-seq in cultured airway epithelial cells.

Total n = 47	Non-smoker controls	Smoker controls	COPD 1	COPD 2	COPD 3–4	
Subjects, n (Female/Male)	9 (8/1)	10 (3/7)	9 (2/7)	10 (0/10)	9 (5/4)	p = 0•001
Age	63 ± 13	61 ± 8	65 ± 6	70 ± 7	63 ± 4	ns
BMI (kg.m^{-2})	23 ± 3	25 ± 3	30 ± 4[*]	28 ± 4	22 ± 4[¶,$]	p<0•001
Smoking history (never /former /current)	9/0/0	0/1/9	0/7/2	0/6/4	0/7/2	p<0•01
Pack-year units	0 ± 0	38 ± 23[*]	49 ± 29[*]	50 ± 15[*]	46 ± 23[*]	p<0•0001
FEV1 pre-bronchodilation (% of PV)	101 ± 18	91 ± 12	91 ± 9	66 ± 10[*,#,¶]	23 ± 11[*,#,¶,$]	p<0•0001
FEV1 post-bronchodilation (% of PV) (n)	74 ± 0 (n = 1)	91 ± 15 (n = 2)	94 ± 12 (n = 6)	69 ± 11[#,¶] (n = 7)	25 ± 13[#,¶,$] ($n$ = 9)	p<0•0001
FEV1 absolute increase after bronchodilation, ml (n)	190 ± 0	85 ± 35	95 ± 99	96 ± 66	56 ± 54	ns
FVC pre-bronchodilation (% of PV)	102 ± 15	95 ± 12	109 ± 13	81 ± 10[*,¶]	57 ± 14[*,#,¶,$]	p<0•0001
FVC post-bronchodilation (% of PV) (n)	92 ± 0 (n = 1)	97 ± 8 (n = 2)	112 ± 12 (n = 6)	90 ± 10 (n = 7)	64 ± 16[#,¶,$] ($n$ = 9)	p<0•0001
FEV1/FVC ratio pre-bronchodilation (%)	79 ± 5	75 ± 4	65 ± 4[*,#]	62 ± 9[*,#]	32 ± 9[*,#,¶,$]	p<0•0001
FEV1/FVC ratio post-bronchodilation (%)	70 ± 0 (n = 1)	76 ± 6 (n = 2)	65 ± 3 (n = 6)	60 ± 9 (n = 7)	32 ± 11[#,¶,$] ($n$ = 9)	p<0•0001
DLCO (% of PV)	91 ± 20	73 ± 9	63 ± 4[*]	61 ± 12[*]	28 ± 11[*,#,¶,$]	p<0•0001
Inhaled corticosteroids, n	0	0	1	1	8	p<0•001
Inhaled corticosteroids mean dosage, μg (BDP equivalent)	NA	NA	400 ± 0	200 ± 0	1438 ± 1131	NA
Inhaled corticosteroids, device (metered-dose inhalers / dry powder inhalers)	NA	NA	0/1	0/1	0/8	NA
Radiological findings						
Bronchiectasis	1/9	1/10	3/9	0/10	3/9	
Emphysema	0/9	5/10	6/9	5/10	9/9	
Mild		2	4	1	1	
Moderate		2	2	2	1	
Severe		1		2	7	
Surgical indication						
Cancer	8/9	9/10	9/9	10/10	2/9	
Adenocarcinoma	5	8	7	4	2	
Squamous	1	1	1	3		
Neuroendocrine	2		1	2		
Other				1		
Non-cancer	1/9	1/10	0/9	0/10	7/9	
Lung transplant					7	
Other	1	1				

Data are presented as mean ± SD, unless otherwise stated. Demographic data, lung function tests, smoking history, and inhaled corticotherapy as well as radiological findings and surgery indication are stated for the patient groups, classified according to smoking history and the presence of airflow limitation. Patients with other lung diseases (*e.g.*, asthma) were excluded from the study.
BDP, beclomethasone dipropionate; BMI, body mass index; COPD, chronic obstructive pulmonary disease; DLCO, diffusing capacity of the lung for CO; FEV1, forced expiratory volume in 1 s; FVC, forced vital capacity; NA, not applicable; PV, predicted values; RNA-seq, RNA-sequencing.
[*] = p<0•05 compared to non-smoker controls.
[#] = p<0•05 compared to smoker controls.
[¶] = p<0•05 compared to COPD stage 1 patients.
[$] = p<0•05 compared to COPD stage 2 patients
ns, not significant.

Table 2
Patient series for total, active and nuclear β-catenin staining.

Total n = 56	Non-smoker controls	Smoker controls	COPD stage 1	COPD stage 2	COPD stage 3–4	
Subjects, n (Female/Male)	7 (3/4)	14 (6/8)	12 (6/6)	12 (4/8)	11 (8/3)	ns
Age	60 ± 8	64 ± 9	65 ± 7	68 ± 10	60 ± 4	ns
BMI (kg.m^{-2})	24 ± 3	27 ± 5	26 ± 6	27 ± 4	23 ± 4	ns
Smoking history (never /former /current /missing)	11/0/0/0	0/4/9/1	0/4/8/0	0/6/6/0	0/11/0 /0	$p<0•01$
Pack-years	0 ± 0	48 ± 17*	57 ± 25*	46 ± 23*	43 ± 14*	$p<0•0001$
FEV1 pre-bronchodilation (% of PV)	108 ± 11	91 ± 16*	88 ± 9*	65 ± 9*,#,¶	19 ± 5*,#,¶,$	$p<0•0001$
FEV1 post-bronchodilation (% of PV) (n)	NA (n = 0)	70 ± 4 (n = 2)	92 ± 10 (n = 10)	67 ± 9 (n = 11)	21 ± 7# (n = 11)	$p<0•0001$
FEV1 absolute increase after bronchodilation, ml (n)	NA (n = 0)	100 ± 0 (n = 2)	77 ± 89# (n = 10)	70 ± 76¶ (n = 11)	22 ± 32#,¶,$ (n = 11)	$p<0•05$
FVC pre-bronchodilation (% of PV)	112 ± 21	95 ± 15	105 ± 12	86 ± 13*,¶	55 ± 13*,#,¶,$	$p<0•0001$
FVC post-bronchodilation (% of PV) (n)	NA (n = 0)	80 ± 3 (n = 2)	110 ± 12 (n = 10)	90 ± 15¶ (n = 11)	58 ± 15¶,$ (n = 11)	$p<0•0001$
FEV1/FVC ratio pre-bronchodilation (%)	79 ± 6	78 ± 6	65 ± 4*,#	60 ± 8*,#	31 ± 7*,#,¶,$	$p<0•0001$
FEV1/FVC ratio post-bronchodilation (%)	NA (n = 0)	83 ± 15 (n = 2)	65 ± 3# (n = 10)	59 ± 9# (n = 11)	32 ± 7#,¶,$ (n = 11)	$p<0•0001$
DLCO (% of PV)	107 ± 14	75 ± 18*	69 ± 19*	57 ± 20*	28 ± 14*,#,¶,$	$p<0•0001$
Inhaled corticosteroids, n	0	0	3	3	11	$p<0•0001$
Inhaled corticosteroids mean dosage, μg (BDP equivalent)	NA	NA	967 ± 896	967 ± 896	1445 ± 787	NA
Inhaled corticosteroids, device (metered-dose inhalers / dry powder inhalers)	NA	NA	0/3	0/3	1/10	ns
Radiological findings						
Bronchiectasis	1/7	0/14	1/12	2/12	1/11	
Emphysema	0/7	5/14	7/12	5/12	11/11	
Mild		4	4	1	1	
Moderate			3	3	2	
Severe		1		1	8	
Surgical indication						
Cancer	7/7	14/14	12/12	12/12	0/11	
Adenocarcinoma	4	9	9	8		
Squamous		3	3	2		
Neuroendocrine	2	2		1		
Other	1			1		
Non-cancer	0/7	0/14	0/9	0/12	11/11	
Lung transplant					11	

Data are presented as mean ± SD, unless otherwise stated. Demographic data, lung function tests, smoking history, and inhaled corticotherapy as well as radiological findings and surgery indication are stated for the patient groups, classified according to smoking history and the presence of airflow limitation. Patients with other lung diseases (*e.g.*, asthma) were excluded from the study. N is specified when data are missing.
BDP, beclomethasone dipropionate; BMI, body mass index; COPD, chronic obstructive pulmonary disease; DLCO, diffusing capacity of the lung for CO; FEV1, forced expiratory volume in 1 s; FVC, forced vital capacity; NA, non applicable; PV, predicted values.
* = $p<0•05$ compared to non-smoker controls.
# = $p<0•05$ compared to smoker controls.
¶ = $p<0•05$ compared to COPD stage 1 patients.
$ = $p<0•05$ compared to COPD stage 2 patients
ns, not significant.

from Ambion with bromochloropropane (BCP) was used instead of chloroform to avoid DNA contamination. RNA quantity was evaluated for each sample with Qubit™ RNA HS Assay Kit (Thermo Fisher Scientific, Waltham, MA). RNA integrity and quality were assessed with an Agilent Bioanalyzer, using the Agilent RNA 6000 Nano kit. We selected 47 amongst the 70 samples, in order to use RNA with a RIN > 9•2 and a DV200 > 90%.

2.3.2. Panel design

Gene expression was evaluated using a TruSeq® custom Targeted RNA Expression kit from Illumina. The design was based on a predesigned gene expression profiling solution from Illumina (TruSeq Targeted RNA Expression WNT Panel; Illumina Inc., San Diego, CA). This panel was designed by Illumina to study WNT signalling pathway and included assays targeting 93 genes. Five other WNT-related genes were added, as well as 8 EMT-related genes and 9 potential housekeeping genes, as recapitulated in Table S2. Moreover, 75 Notch-related and 21 epithelium-related genes were added to the panel but dedicated for a separated analysis. Thus, amongst these 211 genes, 115 genes were investigated and allocated into two separated panels according to their expression level (lowly or highly expressed).

2.3.3. Next generation sequencing (NGS)

The library preparation was performed using 50 ng total RNA, according to the manufacturer's protocol (#15,034,665 v01, January 2016). The first cDNA strand synthesis was performed following the CDNASYN1 program for intact total RNA. Targets were amplified using 30 and 32 cycles for the lowly and highly expressed genes panels, respectively. The quality of the final libraries was controlled with an Agilent Bioanalyzer, using the Agilent DNA 1000 kit, and samples were equimolarly pooled (4 nM). The pooled libraries were then diluted to 15pM and 10pM (for the lowly and highly expressed genes panels, respectively), and loaded on a MiSeq Reagent Kit v3 (Illumina Inc.). The libraries were sequenced using 51 cycles single-read.

2.3.4. Statistical analysis

RNA-seq data analysis was performed separately for each panel (lowly and highly expressed genes), according to the following bioinformatics pipeline. Reads were aligned to the sequences of the targeted transcript retrieved from the human reference genome (UCSC assembly hg19) using BWA (v.0.7.17). Samtools (v.1.9) was used to generate, to sort and to index the BAM files. Read counting for each transcript was performed with the Genomic Alignments (v.1.36.0) Bioconductor package. The geNorm algorithm implemented within the ctrlGene (v.1.0.1). R package was used to identify stably expressed genes amongst the set of measured housekeeping genes. The selected housekeeping genes were used within the DESeq2 (1.24.0) Bioconductor package in order to compute the size factors associated with each library. The DESeq2 package was then used to estimate fold-changes and p-values for each transcript between

Table 3
Patient series for microdissection.

Total n = 12	Non-smoker controls	COPD stage 4	
Subjects, n (Female/Male)	6 (4/2)	6 (5/1)	ns
Age	59 ± 9	58 ± 4	ns
BMI (kg.m^{-2})	27 ± 6	24 ± 5	ns
Smoking history (never /former /current)	6/0/0	0/6/0	p<0•001
Pack-years	0 ± 0	38 ± 12	p<0•01
FEV1 pre-bronchodilation (% of PV)	91 ± 15	22 ± 8	p<0•01
FEV1 post-bronchodilation (% of PV)	NA	24 ± 8	NA
FEV1 absolute increase after bronchodilation, ml	NA	52 ± 73	NA
FVC pre-bronchodilation (% of PV)	97 ± 13	62 ± 11	p<0•01
FVC post-bronchodilation (% of PV)	NA	67 ± 10	NA
FEV1/FVC pre-bronchodilation ratio (%)	77 ± 6	45 ± 16	p<0•01
FEV1/FVC post-bronchodilation ratio (%)	NA	42 ± 15	NA
DLCO (% of PV)	89 ± 24	28 ± 17	p<0•01
Inhaled corticosteroids, n	0	4	p<0,05
Inhaled corticosteroids mean dosage, μg (BDP equivalent)	NA	950 ± 900	NA
Inhaled corticosteroids, device (metered-dose inhalers / dry powder inhalers)	NA	0/4	NA
Radiological findings			
Bronchiectasis	0/6	1/6	
Emphysema	0/6	6/6	
Mild			
Moderate		1	
Severe		5	
Surgical indication			
Cancer	6/6	0/6	
Adenocarcinoma	2		
Squamous			
Neuroendocrine	2		
Other	2		
Non-cancer	0/6	6/6	
Lung transplant		6	

Data are presented as mean ± SD, unless otherwise stated. Demographic data, lung function tests, smoking history, and inhaled corticotherapy as well as radiological findings and surgery indication are stated for the patient groups, classified according to smoking history and the presence of airflow limitation. Patients with other lung diseases (*e.g.*, asthma) were excluded from the study.
BMI, body mass index; COPD, chronic obstructive pulmonary disease; DLCO, diffusing capacity of the lung for CO; FEV1, forced expiratory volume in 1 s; FVC, forced vital capacity; PV, predicted values.
ns, not significant.

group of interest (*e.g.* COPD1 *versus* non-smoker controls, COPD2 *versus* non-smoker controls, ...). Multiple testing correction of the p-value was performed within DESeq2 by the Benjamini-Hochberg procedure [42] in order to control the false discovery rate (FDR) at a level of 0•10. Accordingly, genes associated with an adjusted p-values < 0•10 were considered significant and were therefore expected to include 10% of false positive results. While less conservative than the Bonferroni's correction, this approach and associated threshold is commonly used in transcriptomic studies and selected here to increase the statistical power. All statistical analyses were performed using R.3.6.1.

Both raw and processed RNA-seq data were deposited on the Gene Expression Omnibus (GEO) and made publicly available (GSE155588).

2.4. Reverse transcriptase quantitative polymerase chain reaction (RT-qPCR) assays

RNA extraction, reverse transcription, and RT-qPCR were performed as previously described [43]. Total RNA was extracted from reconstituted ALI-cultured epithelia using TRIzol reagent (Thermo Fisher Scientific). 500 ng of RNA was reverse-transcribed with RevertAid H Minus Reverse transcriptase kit with 0•3 μg of random hexamer, 20 U of RNase inhibitor and 1 mM of each dNTP (Thermo Fisher Scientific) following the manufacturer's protocol in a thermocycler (Applied Biosystems, Foster City, CA). The expression levels were quantified by real-time quantitative PCR using the CFX96 PCR (Bio-Rad, Hercules, CA). The reaction mix contained 2•5 μl of complementary desoxyribonucleic acid diluted 10-fold, 200 nM of each primer (primers properties are detailed in Table S3) and 2x iTaq UniverSybr Green® Supermix (Bio-Rad) in a final volume of 20 μl. The cycling conditions were 95 °C for 3 min followed by 40 cycles of 95 °C for 5 s and 60 °C for 30 s. To control the specificity of the amplification products, a melting curve analysis was performed. The copy number was calculated from the standard curve. Data analysis was performed using Bio-Rad CFX software (Bio-Rad). Expression levels of target genes were normalized to the geometric mean of the values of the 3 housekeeping genes (RPL27, RPS13, RPS18).

2.5. Western blot assays

HBEC lysates were analysed by Western blot as previously described [44], except for band revelation (see below). Cells were lyzed with 150 μl of Laemmli's sample buffer containing 0•7 M 2-mercaptoethanol (Sigma-Aldrich) and lysates were stored at −20 °C. After thawing, samples were heated at 100 °C for 5 min, loaded in a SDS-PAGE gel before migration at 100 V for 15 min and then at 180 V for 50 min. Cell proteins were transferred onto a nitrocellulose membrane (Thermo Fisher Scientific) at 0•3A for 2 h 10 min at RT. The membranes were blocked with 5% w/v BSA (Sigma-Aldrich) in TBS with 0•1% Tween 20 (Sigma-Aldrich) for 1.5 hour at RT, then washed and incubated overnight at 4 °C with a primary antibody according to the target protein (see Table S4 listing used primary and secondary antibodies). Membranes were then incubated for 1 hour at RT with horseradish peroxidase (HRP)-conjugated secondary anti-rabbit (Cell Signalling, Danvers, MA) or anti-mouse (Sigma) immunoglobulin G (IgG). Immunoreactive bands were revealed by chemiluminescence (GE Healthcare, Pittsburgh, PA), detected by Chemidoc XRS apparatus (Bio-Rad) and quantified using the Quantity One software (Bio-Rad).

2.6. Immunohistochemistry, image acquisition and analysis

Samples were processed as previously described [45]. Lung samples were fixed in 4% formaldehyde and embedded in paraffin wax. Sections were deparaffinised in toluene and rehydrated through a graded series from methanol to water, then underwent antigen retrieval treatment using cooker pressure treatment at 15 pound-force per square inch (PSI) for 5 min. Endogenous peroxidase, biotin and streptavidin sites were inactivated by hydrogen peroxide and Bloxall (Vector Laboratories Inc., Burlingame, CA). Nonspecific protein binding sites were blocked with goat serum (Abcam Inc., Cambridge, MA) for 1 h. Primary antibodies were incubated overnight at 4 °C. Mouse IgG_1 or rabbit IgG isotype were used as negative controls, according to the primary antibody species and to their concentration. After washes with TBS 0•1% Tween 20, sections were incubated with goat anti-rabbit or anti-mouse polyHRP-conjugated IgG. Table S4 recapitulates the primary and secondary antibodies that were used. Revelation was performed by using 3,3′-Diaminobenzidine (DAB) (Sigma-Aldrich). Sections were counterstained with Hematoxylin (Sigma-Aldrich) and coverslipped. Images were acquired with Leica SCN400 slide scanner (Leica Biosystems, Newcastle, United Kingdom).

After manual delineation of the AE (10 fields per slide, 20x magnification), quantification was selectively performed on these zones with Leica software (Leica Biosystems). "% of positive area" states for the percentage of the epithelium surface displaying a stronger staining than the determined threshold. "Staining concentration" is defined as the measure of the concentration of the stain within the delineated tissue area. The staining concentration is calculated using the following formula:

$$Concentration = \frac{\sum_{i=0}^{i=31}[h(i) * absorbance\ (i)]}{TotalTissuePixels} * 10,000, \quad \text{with } Absorbance = -\ln\frac{(i * 8 + 4)}{TissueThreshold}$$

where i is an intensity bin number from 0 to 31; h(i) is the number of positive pixels with intensity i, absorbence (i) is the absorbence at intensity i; Total Tissue Pixels is the total number of tissue pixels in the delineated analysis area; Tissue Threshold is the input tissue threshold intensity.

2.7. Immunofluorescence staining using tyramide signal amplification

Five micron-sections of lung tissue or reconstituted ALI epithelium, fixed in 4% formaldehyde and paraffin-embedded, were deparaffinised in toluene and rehydrated through a graded series from ethanol to water. Antigen retrieval was performed in citrate buffer (pH 6•0 containing 0•1% of triton) using a pressure cooker at 15 PSI for 5 min. Sections were blocked for non-specific antigen binding by incubation in Bloxall (Vector Laboratories Inc.) for 15 min and then in 0•3% hydrogen peroxide with 5% goat serum (Bio-Rad) for 30 min. Staining first included a 30 min protein blocking with 5% goat serum, then the primary antibodies diluted in 5% normal goat serum solution were applied, then the appropriate SuperBoost™ goat anti-rabbit or anti-mouse, poly-HRP-conjugated secondary antibody (Thermo Fisher Scientific) was applied for 40 min. HRP-conjugated polymer mediated the focal covalent binding of a fluorophore using tyramide signal amplification. Table S5 recapitulates the antibodies and fluorophores that were used. Finally, sections were counterstained with Hoechst (Thermo Fisher Scientific) diluted at 10 μg/ml in TBS-BSA 5% and mounted with Dako fluorescence mounting medium (Dako, Carpinteria, CA). For negative controls, we used rabbit or mouse isotype controls at the same concentration as the corresponding primary antibodies (diluted in 5% normal goat serum).

2.8. Laser capture microdissection

Optimal Cutting Temperature (OCT)-embedded proximal bronchial tissue from non-smoker controls (n = 5) and very severe COPD patients (n = 6) was selected. The day before microdissection, 20 μm thick sections were obtained, in RNase-free conditions on a microtome-cryostat (cryochamber temperature, −20 °C). Sections were disposed on polyethylene naphtalate (PEN) Membrane Frame Slides (Thermo Fisher Scientific) and stored at −80 °C. Less than an hour before microdissection, sections were dehydrated in graded ethanol solutions, stained with cresyl violet (Ambion) and fixed with xylene. Epithelial microdissection was performed using the Leica LMD 6000. RNA was extracted from microdissected samples as previously described [43]. Detailed information on sample preparation, staining and microdissection is provided elsewhere [46].

2.9. Enzyme-linked immunosorbent assay (ELISA)

Secretory component (SC) concentration was determined in apical washes by sandwich ELISA, as previously described [45]. Fibronectin basolateral release was assessed as previously described [40]. Total TGF-β_1 concentration in basolateral supernatants was measured according to manufacturer's instructions (Bio-Techne, Minneapolis, MN). Briefly, 96-well plates were first coated overnight, at 4 °C, with anti-fibronectin, -TGF-β_1, or -SC antibodies diluted in bicarbonate buffer (pH 9•6). Then, after blocking with phosphate-buffered saline BSA 1% for 90 min at 37 °C, HBEC apical washes (for SC) or basolateral supernatants (for fibronectin and total TGF-β_1) were incubated for 60 min at 37 °C, along with standard samples. Detection was performed with a first incubation with the corresponding biotinylated antibody (anti-fibronectin, -TGF-β_1, or -SC), followed by a second incubation with HRP-linked anti-mouse IgG, for 1 h each. Revelation was performed with 3,3′,5,5′-tetramethylbenzidine and stopped with H2SO4 1.8 M.

2.10. Statistical analysis

Results were analysed with JMP® Pro, Version 14 (SAS Institute Inc., Cary, NC) and GraphPad Prism version 8.0.2 (GraphPad Software, La Jolla, CA), and were expressed as medians and interquartile ranges. p-values $<$ 0•05 were considered statistically significant.

3. Results

3.1. WNT/β-catenin pathway is upregulated in ex-vivo reconstituted COPD proximal AE

ALI-HBEC constitute a model in which epithelial cells recapitulate, *in vitro*, several features of the native epithelial phenotype as observed *in situ* [40,47], therefore allowing to focus on epithelial pathobiology whilst avoiding mesenchymal (including leucocytes) contamination. This approach is particularly relevant to WNT signalling, as surrounding mesenchymal cells strongly express WNT and could) interfere with the resulting bulk data. Whether the canonical WNT pathway is activated in the bronchial epithelium in COPD was thus assessed by targeted RNA-sequencing (RNA-seq) of reconstituted AE (analysed at 2 weeks of ALI-culture, a time window of active differentiation) from 47 samples originating from 5 groups: non-smoker controls (n = 9), smoker controls (n = 10), mild COPD (n = 9), moderate COPD (n = 10), and (very) severe COPD (n = 9). The characteristics of the study population are summarized in Table 1. A total of 115 genes was studied, including 98 selected WNT-related genes. As WNT signalling has been recently linked with EMT [28,29,48], possibly through TGF-β signalling [28], we also selected 8 EMT and TGF-β-related genes. Finally, 9 potential housekeeping genes were assessed. The expression of all 115 genes was measured by using a

MiSeq™ Sequencing Platform, and each group was compared to non-smoker controls. A second analysis, comparing pooled COPD patients with non-smoker controls, was performed separately (see below).

The RNA-seq showed a significant dysregulation of 25 genes of the panel, involving several components of the WNT pathway. Increased expression of the WNT receptor *FZD7* was observed as well as of the β-catenin gene (*CTNNB1*), cytoplasmic and nuclear WNT pathway components (*CD44, CSNK2A1, CSNK2A2, FBXW11, TCF7L1, SOX4*), and WNT downstream targets including components of other pathways (*TGFB2, TGFBR1, TGFBR2, EGFR, IL6, VEGFA*), EMT-related proteins (*VIM, FN1*), matrix metalloproteinases (*MMP2, MMP7*), and cell cycle-related proteins (*JUN, CCND1*). Conversely, WNT inhibitors *CTNNBIP1, RUVBL1* and *SOX2* were consistently downregulated. These changes prevailed in severe COPD, as shown in the heat map recapitulating the most affected genes (Fig. 1a) and in volcano plots allowing the comparison between each group with non-smoker controls (Figure S1). A complete heat map listing all the genes that were studied is provided in the supplementary data (Figure S2). This picture is consistent with canonical WNT activation in the COPD AE, in particular in patients with severe disease, as schematized in Fig. 1b. The most affected target genes (> 2-fold change) in RNA-seq, namely *MMP2, MMP7, FZD7, SOX4*, as well as *CTNNB1*, the cardinal factor of canonical WNT, were validated by RT-qPCR. As qPCR was expected to be less sensitive than RNA-seq, the initial 47 patients series used for RNA-seq was enriched with 21 additional samples (also from 2 weeks ALI cultures); clinical characteristics of the resulting 68 patients are shown in Table S1. Upregulation of *MMP2* and *MMP7* was confirmed in all COPD groups, while *FZD7* and *SOX4* expression was increased when pooling COPD patients (Fig. 1c). Although *CTNNB1* was not significantly upregulated, these data globally validated RNA-seq data and activation of WNT/β-catenin pathway in the COPD airway epithelium.

3.2. β-catenin expression is increased in the COPD AE

The canonical WNT pathway depends on the nuclear accumulation of the transcriptional co-activator β-catenin. Therefore, for both total and active (non-phosphorylated) β-catenin, we stained bronchial sections from 56 patients divided into 5 groups (as for RNA-seq): non-smokers (n = 7), smoker controls (n = 14), mild COPD (n = 12), moderate COPD (n = 12), and (very) severe COPD (n = 11). The population characteristics are detailed in Table 2.

Firstly, the expression of total β-catenin protein was increased in the proximal AE of patients with very severe COPD, compared with non-smokers and smoker controls, in terms of both percentage of stained area (Fig. 2a) and staining concentration (Figure S3a). Accordingly, the increase in β-catenin expression correlated with airflow limitation depicted by decreased FEV_1 (Fig. 2b and S3b). Secondly, the immunostaining for active (non-phosphorylated) β-catenin was increased in the large AE of patients with severe COPD compared with non-smokers and smoker controls, in terms of percentage of stained area (Fig. 2d) and staining concentration (Figure S3c), and also correlated modestly with airflow limitation (Fig. 2e and S3d). Representative pictures of staining for total and active β-catenin in non-smoker controls and very severe COPD epithelium are shown in Figs. 2c and 2f.

As active β-catenin includes nuclear and junctional β-catenin, nuclear active β-catenin was quantified separately, demonstrating that severe COPD patients displayed more positive β-catenin nuclei than non-smokers and smoker controls (Fig. 2g), which significantly correlated with disease severity (Fig. 2h). Increased nuclear expression of β-catenin was also observed in the *ex-vivo* ALI-reconstituted epithelium from a series of 22 COPD patients, as compared to 19 controls (Figure S4), further demonstrating the replication of the original phenotype by this model.

In order to confirm WNT/β-catenin activation in the proximal AE in COPD, laser microdissection was used in lung tissue sections from non-smoker controls and severe COPD patients (n = 6 per group) to selectively assess key WNT-related gene expression at the AE level, while avoiding the interference of WNT expression by surrounding, non-epithelial tissues (Fig. 3a). The clinical characteristics of this patient series are summarized in Table 3.

AXIN2, CTNNB1, SOX4, TCF7L2 and *FZD7* genes were upregulated in the COPD epithelium as compared with controls (Fig. 3b), while trends for upregulation were observed for *MMP2* and *MMP7*.

3.3. β-catenin upregulation in COPD AE correlates with altered differentiation

We next explored whether the increased β-catenin expression observed *in situ*, in the COPD proximal AE, could be linked with differentiation abnormalities such as lineage changes (basal, ciliated and secretory/goblet cell numbers). Data from a previous study from our laboratory [6], where bronchial sections were stained for basal, ciliated and goblet cells markers (p63 – Forkhead Box J1 [FOXJ1] – and MUC5AC, respectively), were extracted for the same 56 patients of this study. In airway tissue from those patients, the COPD proximal AE displayed decreased numbers of ciliated cells and increased numbers of goblet cells, as compared with non-smokers and smoker controls (Fig. 4a and 4d). Both changes correlated modestly but significantly with total and active β-catenin staining (Fig. 4b-c and e-f), suggesting that WNT activation in COPD is linked with differentiation abnormalities. In contrast, no change in basal cell numbers was observed (Fig. 4g). Representative pictures of FOXJ1 and MUC5AC staining in non-smoker controls and very severe COPD AE are shown in Fig. 4h-i.

3.4. WNT/β-catenin activation contributes to epithelial pathology in COPD airways

Following the demonstration that WNT/β-catenin is activated in the COPD AE, both *in vitro* and *in situ*, it was next assessed whether the modulation of the WNT/β-catenin pathway during epithelial redifferentiation could influence the expression of COPD-related features such as altered polarization and barrier function, lineage specification, and EMT. To this aim, the ALI-reconstituted epithelium from 6 very severe COPD patients was treated at different time-periods of the redifferentiation (after ALI D1–5, during which modulation completely suppressed epithelial growth, *not shown*) with a specific canonical WNT activator (CHIR99021, 10 μM) or inhibitor (XAV939, 10 μM) as compared to vehicle control (DMSO). First, it was confirmed that CHIR99021 activates and XAV939 inhibits the canonical WNT pathway; CHIR99021 induced at each time-period a sharp increase in active β-catenin protein level (Figure S5a-b) and in *AXIN2* gene expression, a good reporter of canonical WNT activation (Figure S5c), although no effect was observed on the expression of the β-catenin gene (*CTNNB1*, Figure S5d). Conversely, XAV939 decreased the active β-catenin protein levels and AXIN2 gene expression (Figure S5a-d). CHIR-induced active β-catenin increase was associated with its translocation from the cell membrane to the nucleus (Figure S5e).

3.4.1. WNT activation alters the early differentiation program of AE cells

WNT activation (induced by CHIR99021) strongly suppressed *MYB* expression at all time-periods, a transcription factor involved in early epithelial differentiation. WNT inhibition (induced by XAV939) had no effects on *MYB* expression at T2, but also inhibited its transcription at T1 and T3, although to a lesser extent than WNT activation (Fig. 5a).

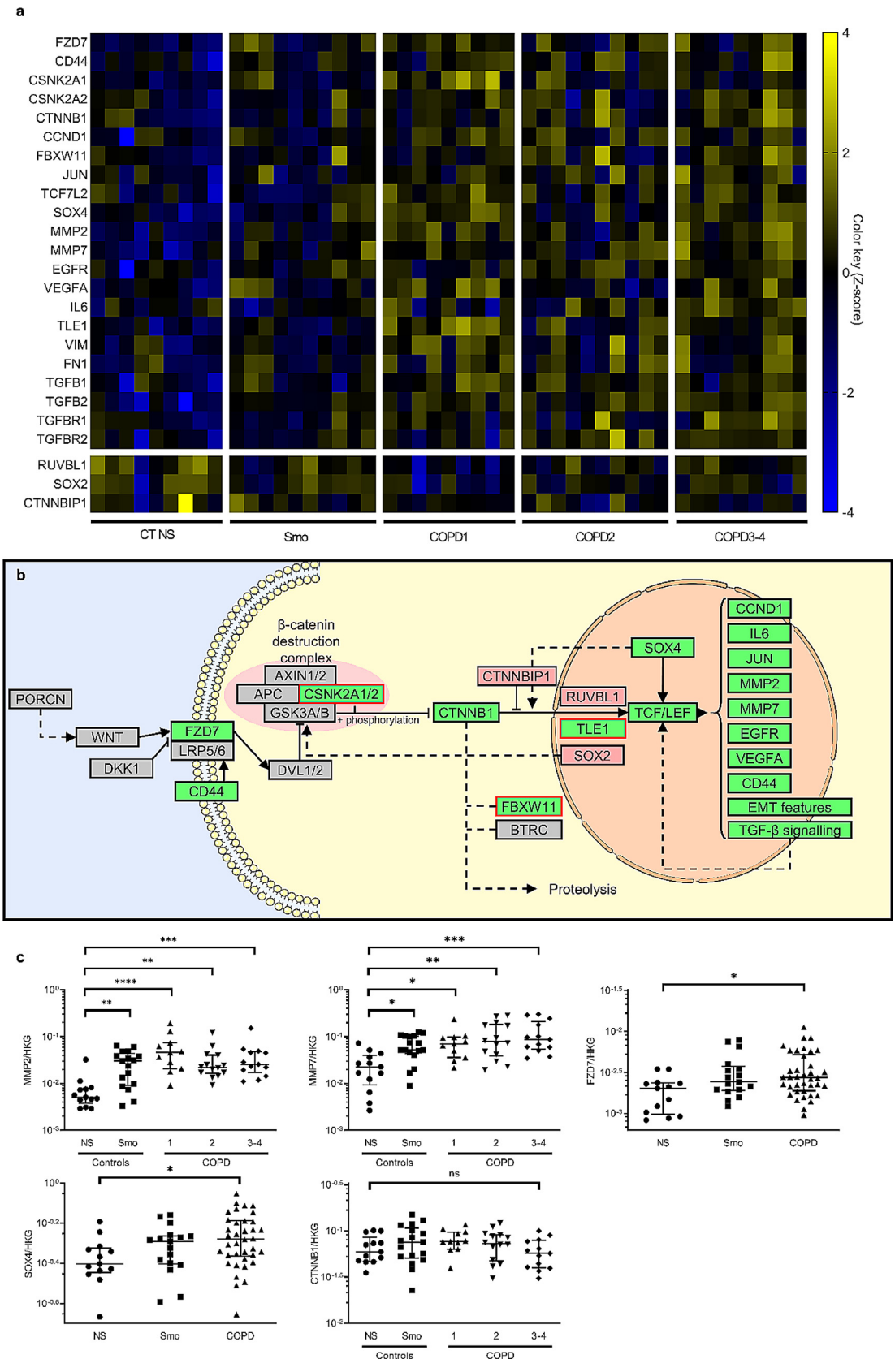

Fig. 1. Canonical WNT pathway is upregulated in COPD proximal epithelium.

a) Heat map of RNA-seq expression Z-score, computed for all significantly modified genes (fold discovery range < 0•1) in smokers and COPD, as compared with non-smoker controls. These results depict a global WNT activation in COPD, that is more pronounced in very severe disease. The horizontal gap separates upregulated and downregulated targets.

b) Schematized overview of the canonical WNT pathway and its most important components. Green and red-filled rectangles respectively represent significantly up- and down-regulated genes in COPD, according to RNA-seq data (dedicated statistical analysis, comparing pooled COPD *versus* non-smoker controls). Red-framed rectangles (*CSNKA1&2,*

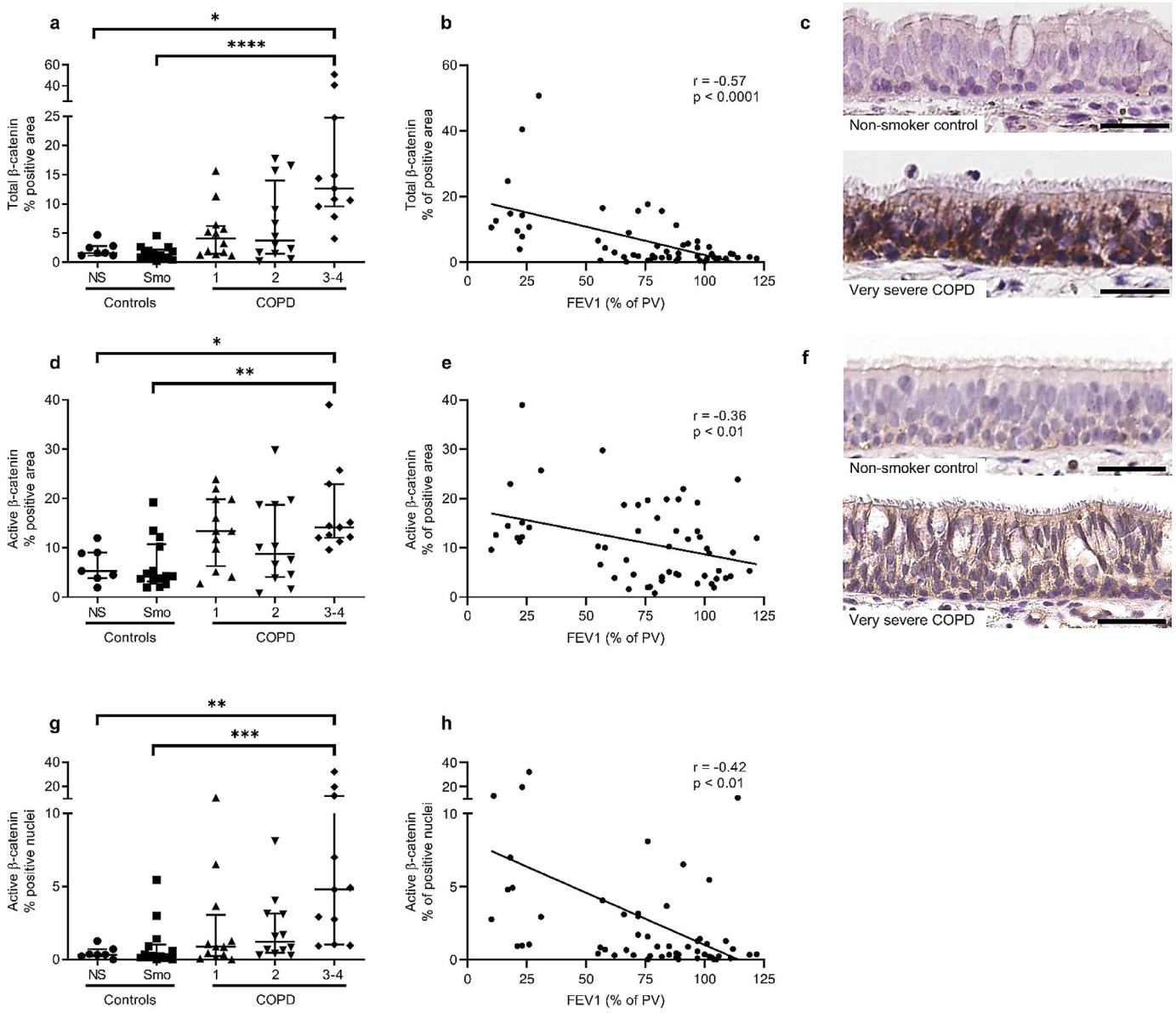

Fig. 2. Total, active and nuclear β-catenin staining is increased in the COPD bronchial epithelium.

a) Total β-catenin staining in the airway epithelium from non-smokers and smoker controls and COPD patients (GOLD classification from 1 to 4 according to the spirometric severity of the disease), in terms of percentage of positive area.

b) Correlation between total β-catenin in terms of percentage of positive area, and disease severity evaluated by the FEV1 (% of predicted values).

c) Representative picture of control and very severe COPD airway epithelium, stained for total β-catenin.

d) Active β-catenin staining was also increased in (very) severe COPD epithelium as compared with non-smokers and control smokers, in terms of percentage of positive area.

e) Correlation between active β-catenin in terms of percentage of positive area, and disease severity evaluated by the FEV1.

f) Representative picture of control and very severe COPD airway epithelium, stained for active β-catenin.

g-h) The percentage of positive active β-catenin nuclei was higher in the epithelium of (very) severe COPD patients as compared with non-smokers and control smokers (g), and correlated with COPD severity witnessed by the FEV1 (h).

*, **, ***, **** indicate p-values of less than 0•05, 0•01, 0•001, and 0•0001, respectively (analysed using the Kruskal-Wallis test followed by Dunn's post-hoc test). Bars indicate median ± interquartile range. COPD, chronic obstructive pulmonary disease; FEV1, forced expired volume in 1 second; NS, non-smokers; Smo, smokers; PV, predicted values. Scale bars, 50 μm.

3.4.2. WNT modulation regulates AE cell specification and commitment

Firstly, goblet cell commitment was assessed by measuring the expression of the SAM Pointed Domain Containing ETS Transcription Factor (*SPDEF*). WNT activation completely suppressed *SPDEF* expression at all time-periods, while WNT inhibition resulted in a 1•5 to 2-fold increase of its transcription (Fig. 5b). Secondly, CHIR99021-induced WNT activation resulted in a marked decrease in Multiciliate Differentiation And DNA Synthesis Associated Cell Cycle

FBXW11, TLE1) point genes whose upregulation does support canonical WNT activation. Interestingly, two of these genes are involved in the phosphorylation and ubiquitination of the β-catenin, and their divergent regulation could be a direct consequence of the increased β-catenin cytosolic pool.

c) The most affected target genes (>2-fold change) in RNA-seq, namely *MMP2, MMP7, FZD7, SOX4*, as well as *CTNNB1*, the cardinal factor of canonical WNT, were validated by RT-qPCR in the initial 47 patients series enriched with 21 additional samples

*, **, ***, **** indicate p-values of less than 0•05, 0•01, 0•001, and 0•0001, respectively (analysed using the Kruskal-Wallis test followed by Dunn's post-hoc test). Bars indicate median ± interquartile range. COPD, chronic obstructive pulmonary disease; EMT, epithelial-to-mesenchymal transition; NS, non-smokers; ns, not significant; Smo, smokers.

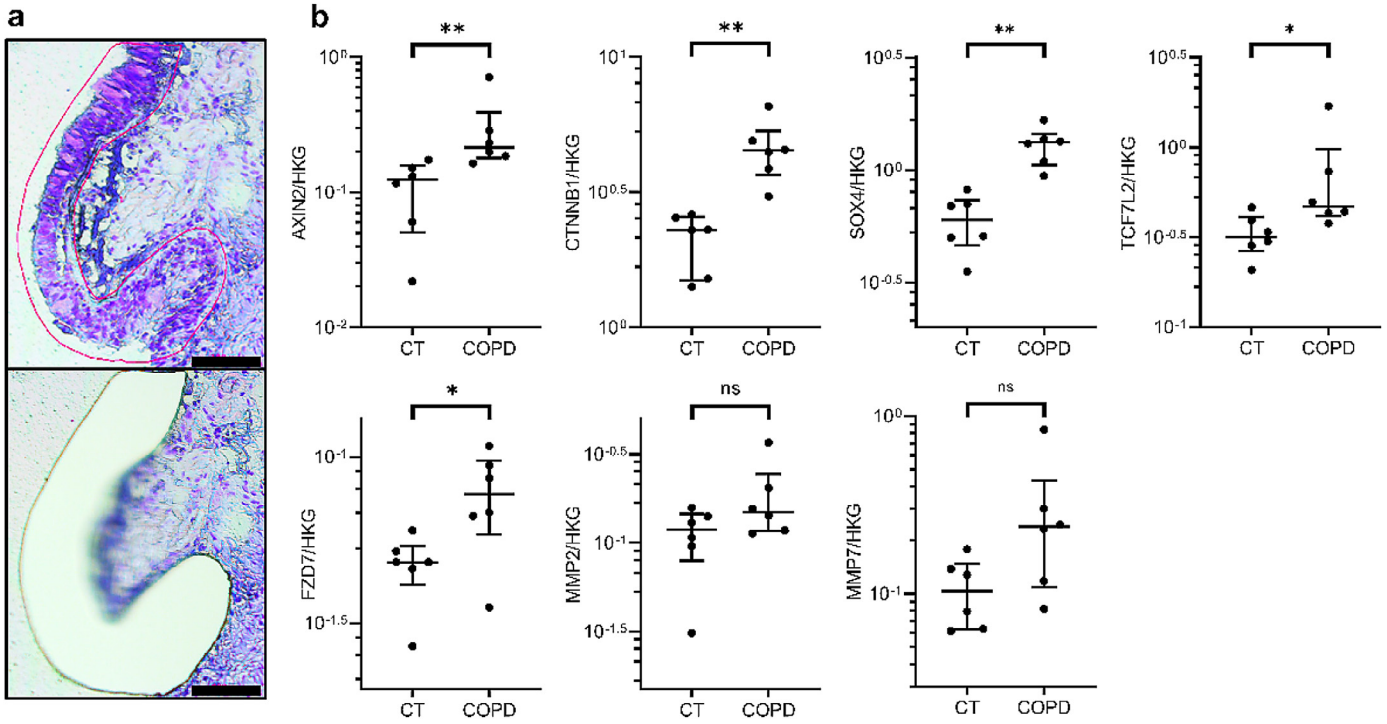

Fig. 3. Canonical WNT pathway is upregulated *in situ* in laser-microdissected COPD airway epithelium

a) Illustrative pictures of the microdissection of the airway epithelium. The upper picture shows the manually delineated epithelium (red line), while the lower picture shows the slide after laser microdissection.

b) Expression of key genes of the WNT/β-catenin pathway (*AXIN2, CTNNB1, TCF7L2, SOX4, and FZD7*) was increased in laser-microdissected epithelium from very severe COPD patients as compared with that of non-smoker controls. Concordantly, upward trends were found for *MMP2* and *MMP7*.

* indicates p-values of less than 0•05 (analysed using the Mann-Whitney test). Bars indicate median ± interquartile range. COPD, chronic obstructive pulmonary disease; CT, controls; ns, not significant. Scale bar, 100 μm.

Protein (*MCIDAS*) expression (Fig. 5c), a transcription regulator involved in the specification of ciliated cells, and almost completely suppressed the transcription of *FOXJ1*, a transcription factor ensuring the commitment towards ciliated cells (Fig. 5d). XAV939-induced WNT inhibition also downregulated *MCIDAS* expression, although to a lesser extent, but upregulated *FOXJ1* at T2 and T3 (Fig. 5c-d). These results indicate that WNT activation inhibits the muco-ciliary programming, and highlight dual effects of WNT inhibition on specification or commitment of ciliated cells, while WNT inhibition favours commitment towards ciliated and goblet cells. In addition, WNT activation also decreased *FOXM1* expression and thus presumably the differentiation towards club cells, which was not significantly affected by WNT inhibition (Fig. 5e). Fig. 5f illustrates CHIR-induced decrease and XAV-induced increase in terminal differentiation proteins of goblet and ciliated cells, respectively MUC5AC and β-tubulin.

3.4.3. *WNT/β-catenin pathway regulates epithelial polarity and barrier function*

WNT activation also alters AE polarization and barrier function. Thus, WNT activation strongly decreases the expression of polymeric immunoglobulin receptor (PIGR, Fig. 6a), a transmembrane protein involved in the basal-to-apical transcytosis of polymeric immunoglobulins at mucosal surfaces and a marker of epithelial polarity. This transcriptional defect was corroborated by a decreased release of the secretory component (SC) in apical washes (Fig. 6b), SC release resulting from the cleavage of the pIgR extracellular part following its baso-apical transcytosis. In addition, CHIR99021 regimen also decreased the expression of tight junction protein 1 (*TJP1*)/Zonula Occludens (ZO)−1 and *CDH1*/E-cadherin 1 (Fig. 6c-f), as key components of epithelial tight and adherens junctions, respectively. Conversely, XAV939-induced WNT inhibition increased *PIGR* (Fig. 6a), *TJP1* (Fig. 6c), and E-cadherin expression (Fig. 6d-f), as well as SC release (Fig. 6b). These results were confirmed by immunofluorescence staining for PIGR and occludin, which were respectively decreased or increased upon WNT activation or inhibition (Fig. 6g).

3.4.4. *WNT modulation regulates the EMT programming*

The modulation of the WNT/β-catenin pathway also regulated EMT programming, indicated by vimentin (gene and protein) expression (Fig. 7a-b and 7d) and fibronectin release (Fig. 7c), which were both increased following WNT activation, while WNT inhibition strongly reduced them (Fig. 7a-d). The awakening of the EMT program in ALI-HBEC probably resulted from the activation of the TGF-β pathway, as phospho-SMAD2 levels paralleled vimentin expression (Fig. 7d-e), and TGF-β_1 basolateral release (but not mRNA transcription) were increased by CHIR99021 (Fig. 7f-g). In contrast, WNT inhibition consistently decreased SMAD2 phosphorylation at T3 (Fig. 7d-e). These results demonstrate an upregulated WNT/TGF-β/EMT axis in the COPD AE, and are consistent with aforementioned RNA-seq findings where COPD patients displayed signals of activation of TGF-β signalling pathway and upregulated EMT-related genes (VIM and FN1) (Fig. 1a).

4. Discussion

This study demonstrates unequivocally, by using cutting-edge RNA-sequencing and laser microdissection of the AE, that the WNT/β-catenin pathway is activated in the proximal bronchial epithelium from patients with COPD. It also highlights that this pathway tightly controls epithelial homoeostasis in the adult lung, canonical WNT activation recapitulating the salient COPD features in the airways such as epithelial de-differentiation, loss of polarity, barrier dysfunction and EMT, while its inhibition reversed the abnormal phenotype of the AE derived from severe COPD patients.

The WNT pathways are ubiquitously involved in foetal development and homoeostasis of several tissues [49]. In the lung, the

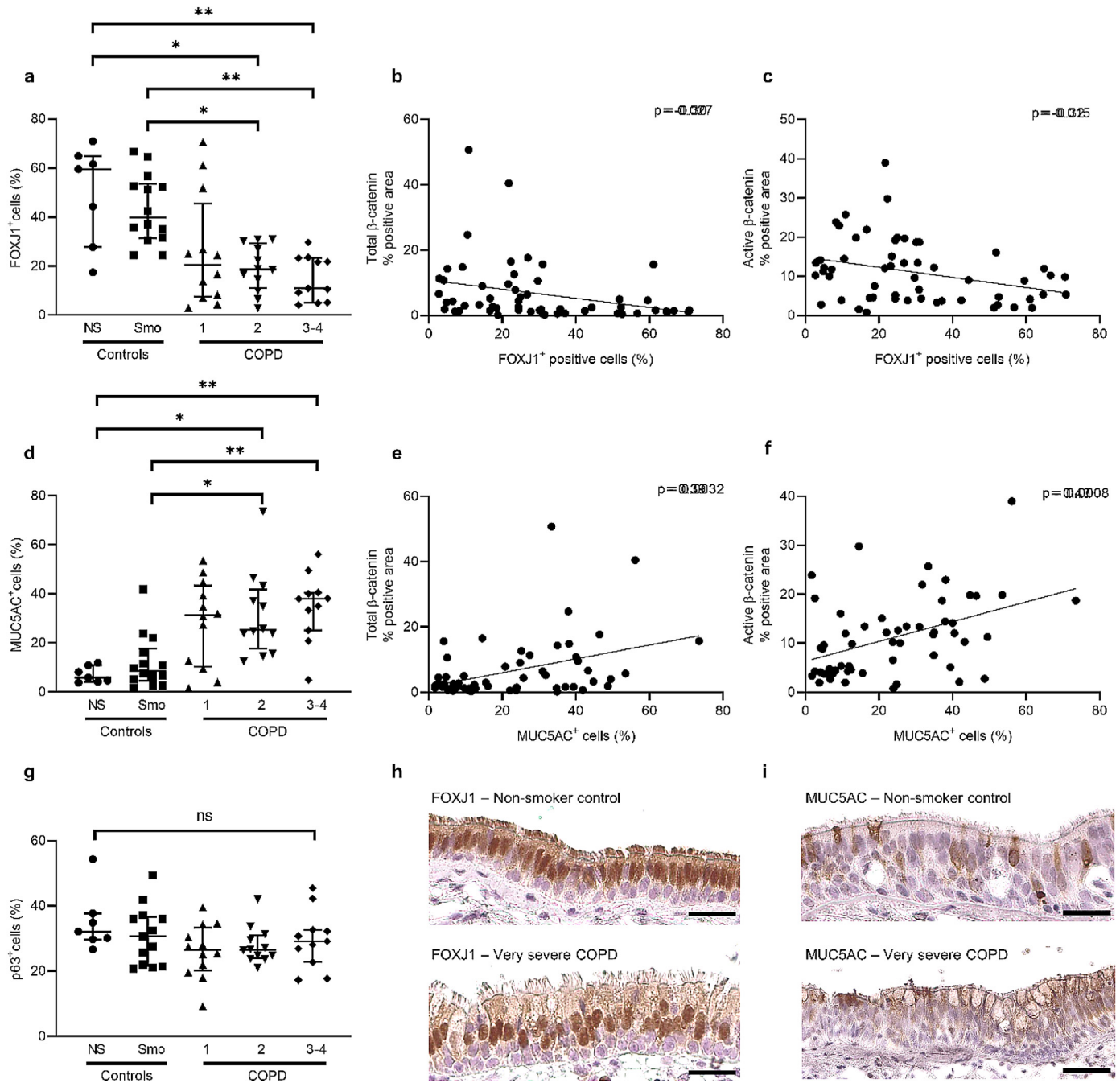

Fig. 4. COPD-related abnormalities in epithelial differentiation.
a) FOXJ1$^+$ cells percentage is decreased in the airway epithelium from COPD2 and COPD3–4 patients, as compared with non-smokers and smoker controls.
b-c) FOXJ1$^+$ cells percentage significantly correlates to both total (b) and active (c) β-catenin staining, in terms of percentage of positive area.
d) MUC5AC$^+$ cells percentage is increased in the airway epithelium from COPD2 and COPD3–4 patients, as compared with non-smokers and smoker controls.
e-f) MUC5AC$^+$ cells percentage significantly correlates to both total (e) and active (f) β-catenin staining, in terms of percentage of positive area.
g) Basal cell populations, assessed by p63$^+$ cells, did not vary in COPD as compared with (non-) smoker controls.
h-i) Representative pictures of FOXJ1 (g) and MUC5AC (h) staining in bronchial sections of non-smoker controls and very severe COPD patients.
*, ** indicate p-values of less than 0•05 and 0•01, respectively (analysed using the Kruskal-Wallis test followed by Dunn's post-hoc test). Bars indicate median ± interquartile range. COPD, chronic obstructive pulmonary disease; NS, non-smokers; Smo, smokers. Scale bars, 50 μm.

importance of WNT signalling in branching morphogenesis and lung growth is well established and its role in AE homoeostasis recently drew scientists' attention [31,50,51]. Previous studies focusing on canonical WNT signalling in the bronchial epithelium highlighted the role of WNT in epithelial differentiation[31] and its regulation by cigarette smoke, as well as its interaction with epithelial inflammation [29,33]. To our knowledge, however, only two recent studies investigated the WNT/β-catenin signalling pathway in COPD at the bronchial tissue level. Wang and colleagues, performing microarrays on small airway samples, found a down-regulation of the canonical WNT pathway in both smokers and COPD [32], while Guo and colleagues described lower β-catenin levels in the epithelium of smokers and COPD patients [33], albeit not specifying whether small and/or large airways were analysed.

In the present study, we specifically studied the proximal AE of healthy non-smokers, healthy smokers and COPD patients, and

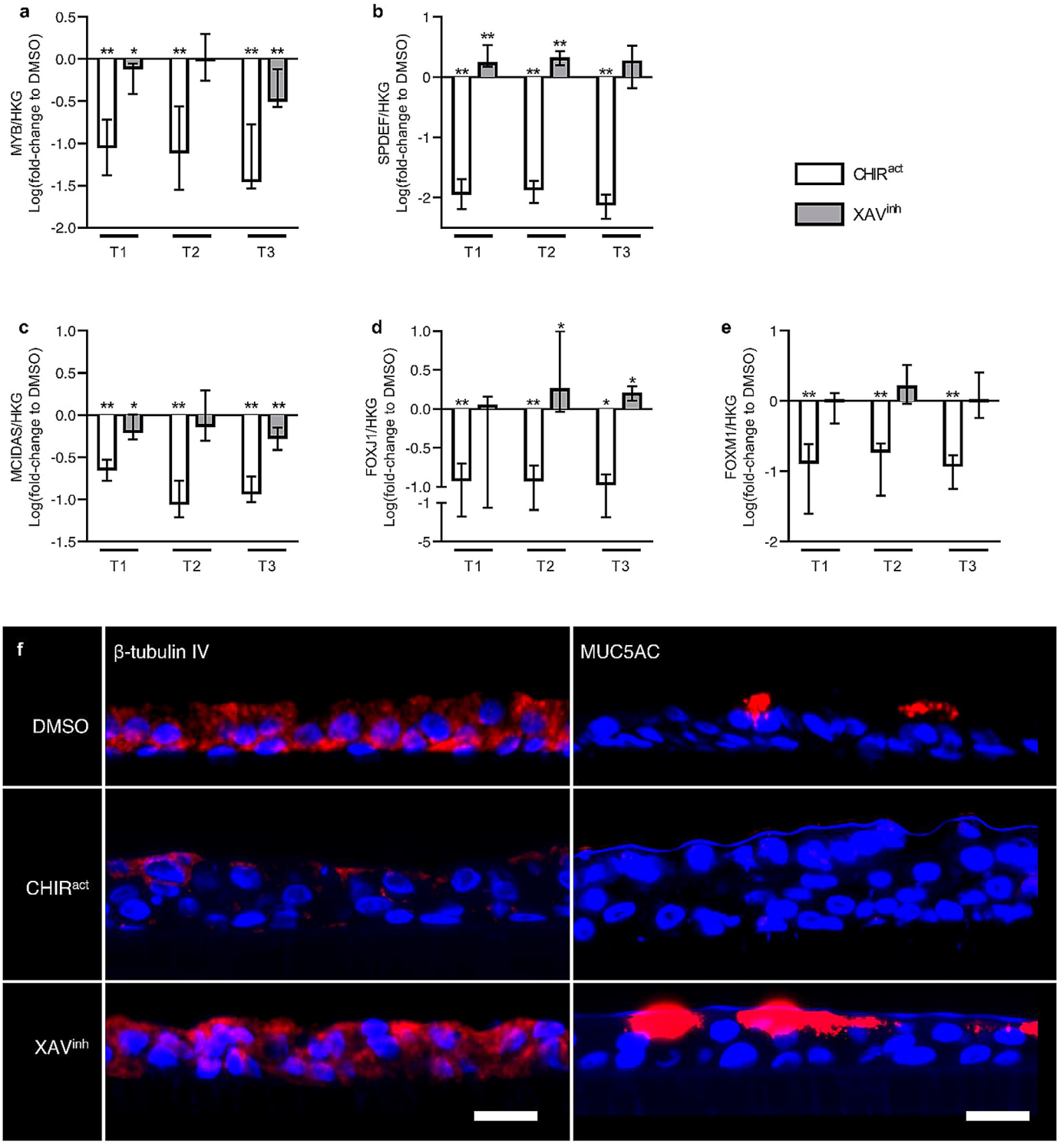

Fig. 5. WNT modulation regulates AE cells differentiation.

a) CHIR99021-induced WNT activation strongly downregulated the expression of *MYB*, an early epithelial differentiation marker, at all time periods. XAV939-induced WNT inhibition also downregulated it at T1 and T3, although in a lesser extent.

b) WNT activation inhibited the commitment towards goblet cells, as *SPDEF* expression was completely suppressed by CHIR99021. Conversely, WNT inhibition increased *SPDEF* expression.

c-d) WNT activation repressed the specification and commitment towards ciliated cells, as CHIR99021 decreased the expression of *MCIDAS* (c) and *FOXJ1* (d). WNT inhibition decreased *MCIDAS* (c) expression but increased *FOXJ1* (d), demonstrating an opposite effect on specification or commitment towards ciliated cells.

e) WNT activation by CHIR99021 decreased the expression of *FOXM1*, a transcription factor involved in the commitment towards club cells, while WNT inhibition by XAV939 had no significant effect.

f) Representative pictures of ALI-reconstituted epithelia, cultured under vehicle condition (DMSO), WNT activation (CHIR99021) or WNT inhibition regimen (XAV939). The epithelium were stained for ciliated cells (β-tubulin IV, left panel) and goblet cells (MUC5AC, right panel), showing a sharp decrease of both cell types upon WNT activation. Conversely, WNT inhibition increased MUC5AC expression and tended to increase β-tubulin IV expression.

*, ** indicate p-values of less than 0•05 and 0•01, respectively (analysed using the Mann-Whitney test). Columns and bars in the graphs represent medians ± interquartile range. Scale bars, 20 μm. CHIR^{act}, CHIR99021-induced WNT activation condition; HKG, housekeeping genes; XAV^{inh}, XAV939-induced inhibition condition.

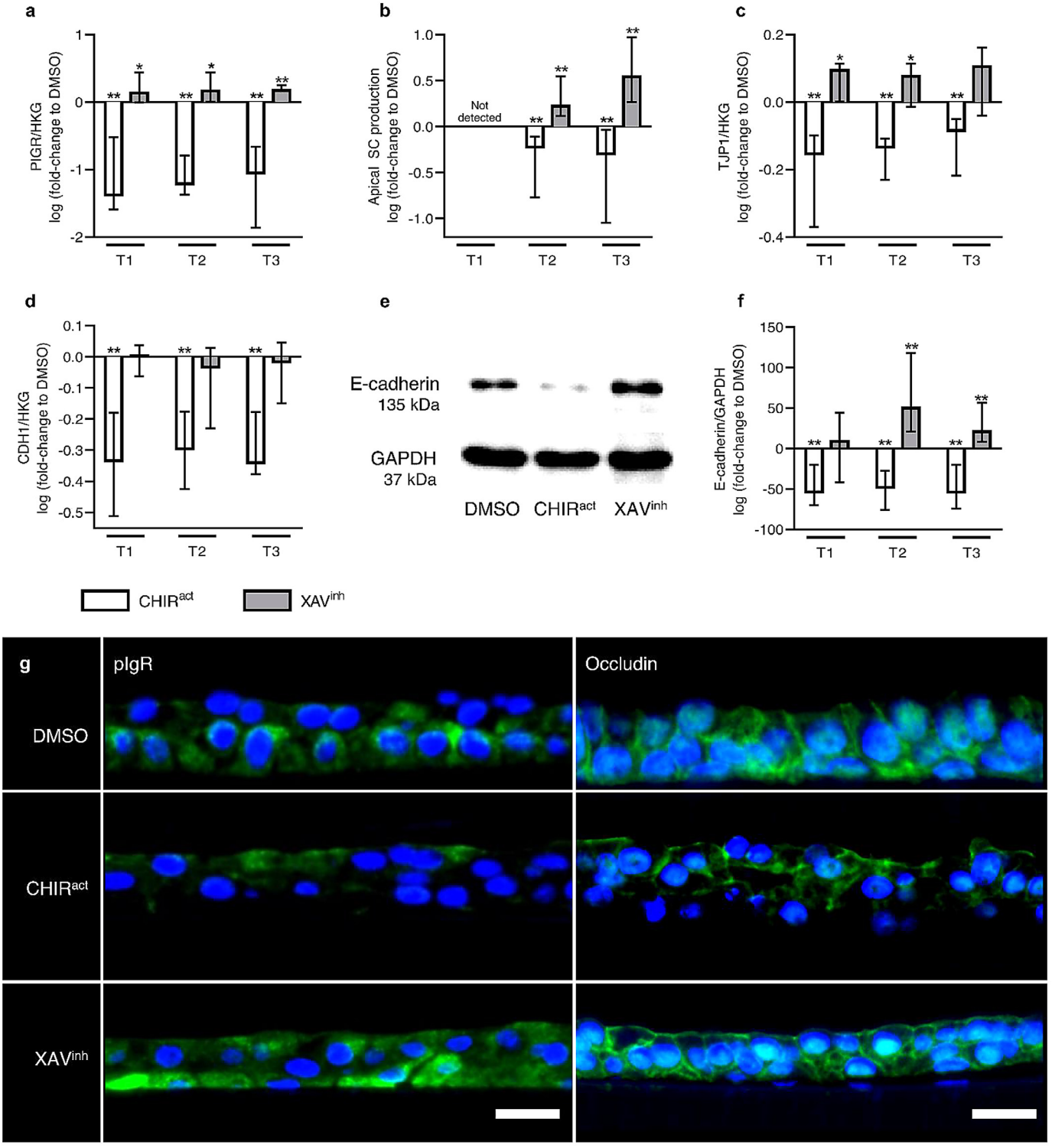

Fig. 6. Canonical WNT pathway regulates AE polarity and barrier function.

a-b) WNT activation impaired *PIGR* gene expression at all time periods (a) and decreased SC release (b), while WNT inhibition increased *PIGR* expression (a) and SC release (b), used as indices of basal-to-apical polarity as this system allows the transcytosis of polymeric IgA and IgM across the epithelial layer.

c-f) CHIR99021-induced WNT activation also decreased the expression of key components of tight and adherens junctions, namely *TJP1* (c) and *CDH1* (d), and resulted in diminished E-cadherin protein levels (e-f), while WNT inhibition increased *TJP1* (c) and E-cadherin (e-f), underscoring the importance of WNT in the epithelial barrier function and tightness.

g) Representative pictures of ALI-reconstituted epithelium, cultured under vehicle condition (DMSO), WNT activation (CHIR99021) or WNT inhibition regimen (XAV939), and immunostained for markers of polarity (pIgR, left panel) and tightness/barrier function (occludin, right panel). WNT activation decreased pIgR and occludin, while WNT inhibition increased pIgR. Occludin staining shows both junctional occludin (cell membrane) and off-target nuclear occludin 1B, an alternatively spliced transcript.

*, ** indicate p-values of less than 0•05 and 0•01, respectively (analysed using the Mann-Whitney test). Columns and bars in the graphs represent medians ± interquartile range. Scale bars, 20 μm. CHIR^{act}, CHIR99021-induced WNT activation condition; HKG, housekeeping genes; XAV^{inh}, XAV939-induced inhibition condition.

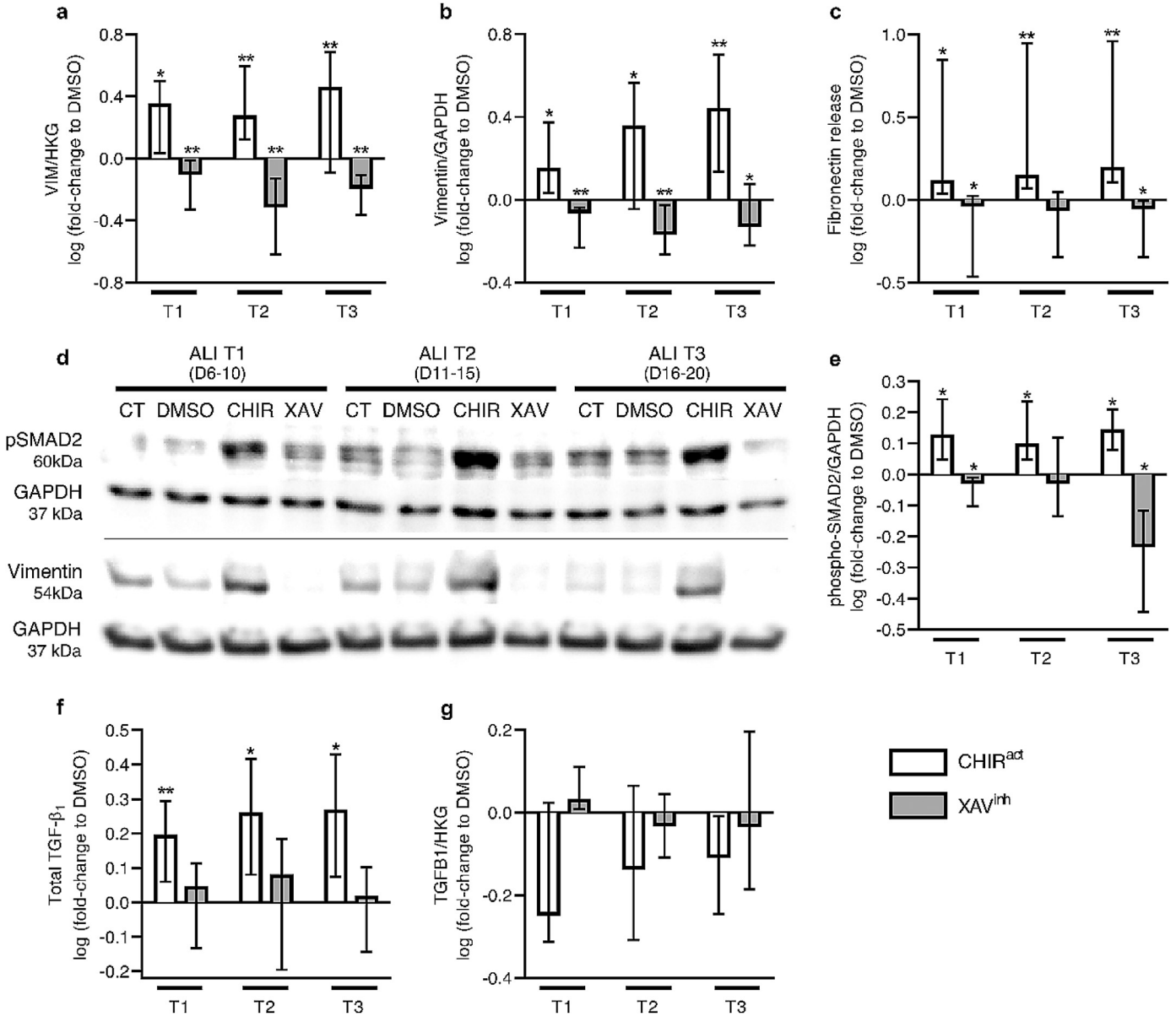

Fig. 7. Canonical WNT activation induces EMT programming.

a-c) WNT activation induced EMT at all time periods, witnessed by the increase in the transcription (a) and protein expression (b) of vimentin, and in the release of fibronectin (c), both being markers of EMT. WNT inhibition, conversely, slightly but significantly decreased them.

d-e) Representative blots for phospho (p)-SMAD2, vimentin, and housekeeping GAPDH proteins (d), and quantitative analysis for phospho (p)-SMAD2, upon control (CT), vehicle (DMSO), WNT activation (CHIR99021), and WNT inhibition (XAV939) conditions (e). In parallel with increased EMT markers, CHIR99021-induced WNT activation increased the phosphorylation of SMAD2, a pivotal component of the canonical TGF-β pathway. In contrast, XAV939 decreased its expression at T1 and T3.

f-g) Concordantly with increased pSMAD2 expression upon CHIR99021-induced WNT activation, TGF-β_1 release in basolateral supernatants was increased in WNT activation conditions (f), whilst no difference was seen upon WNT inhibition. No difference was observed at the transcriptional level (g).

*, ** indicate p-values of less than 0•05 and 0•01, respectively (analysed using the Mann-Whitney test). Columns in graphs represent medians. ALI, air/liquid interface; CHIR^{act}, CHIR99021-induced WNT activation condition; CT, control; HKG, housekeeping genes; XAV^{inh}, XAV939-induced inhibition condition.

demonstrated in a targeted RNA-seq that the WNT/β-catenin pathway is activated at this level in COPD. This observation in the *in vitro*, differentiating epithelium was confirmed *in situ*, in the steady-state epithelium, with upregulated expression of β-catenin and transcription of central WNT elements in surgical samples and microdissected AE from COPD, respectively. ALI-reconstituted and laser-microdissected epithelium allowed to avoid mesenchymal cell contamination, hence to study WNT canonical pathway at the epithelial level only. Interestingly, the increase in epithelial (active) β-catenin by immunochemistry correlated with the COPD severity witnessed by the FEV1, consistently with the RNA-seq data where the sharpest WNT upregulation was found in severe disease. In contrast with previous *in vitro* studies[29,33] where cigarette smoke exposure directly regulated the WNT pathway, no striking changes were observed in smokers without COPD, *e.g.* no increase in β-catenin (or when comparing former *versus* active smokers, not shown), except for *MMP2/7* expression which could relate to other upstream pathways. This discrepancy could relate to differences in sampling, experimental design and/or readouts for analysis. Thus, these studies either focus on small airway epithelium, where signalling pathways might be differently regulated by cigarette smoke, or used 16HBE cells in submerged cultures. Interestingly, it has been suggested that proximal-to-distal patterning in the airways results in different architecture, cell composition, and signalling [52]. In contrast to our findings in the proximal AE, downregulation of the canonical WNT pathway has been documented in COPD at the alveolar level, underlying

emphysema [21-23]. The dual dysregulation of WNT in proximal *versus* distal/alveolar epithelium is to some extent reminiscent of findings regarding TGF-β which are underlying contrasting features of matrix deposition in the airways (airway fibrosis) or matrix disruption in alveoli (emphysema) [53].

AE differentiation, homoeostasis, and repair are complex processes requiring close interactions between developmental pathways such as WNT [31,49], Notch [54-57], and Sonic Hedgehog [58]. It was recently shown that increased β-catenin signalling decreased the number of fully differentiated ciliated cells, while its inhibition increased specification towards ciliated cells [31,50]. Corroborating these findings, we observed that the COPD-related decrease in ciliated cell numbers and increase in goblet cells correlated with increased levels of total and active β-catenin, which display a multicellular pattern in the airway epithelium. However, the differences in WNT signalling highlighted in the RNA-seq data were observed in the differentiating epithelium (active stage of differentiation at 14 days of ALI culture). Thus, whether increased WNT activity relates to changes in (basal, goblet/ciliated) cell numbers (and inherent differences in WNT activity) or to increased signalling activation *per se* remains uncertain. Taking into account previous studies showing that WNT activity is similar between goblet and ciliated cells[59] and that this study (Fig. 4g) as well as our previous study[6] showed unchanged $p63^+$ basal cell numbers (in COPD ALI epithelium and lung tissue), it is likely that WNT upregulation in the airways from COPD patients takes place in basal cells. This is in line with a recent study showing that WNT activation in the airway epithelium at the steady state seems restricted to basal cells [59].

In our study, the specific activation of the pathway (by CHIR99021) during the redifferentiation of the adult human AE completely suppressed the differentiation towards ciliated cells evidenced by the downregulation of *MCIDAS* and *FOXJ1*. In contrast, we also show that extrinsic WNT activation suppresses goblet cell differentiation, in line with the observation that β-catenin destabilization in normal epithelium prevented goblet cell specification during early differentiation period [31]. Conversely, constitutive β-catenin activation in transgenic mice induced goblet cell hyperplasia [60], suggesting either differences due to the model (*e.g.*, murine *vs* human epithelium, constitutive *vs* induced activation) or that WNT could also have dual effects on goblet cell differentiation according to the context. Finally, our data reveal that *FOXM1* is downregulated following WNT activation, presumably affecting differentiation into club cells, and suggesting that in the airways, WNT/β-catenin signalling globally regulates epithelial lineage specification to both ciliary and secretory cell types.

Epithelial barrier dysfunction in the airways may lead to the disruption of apical junctional complexes and the release of active β-catenin from adherens junctions towards the cytosol [61], resulting in WNT/β-catenin activation. It remained however unclear whether, in turn, WNT activation could promote epithelial barrier dysfunction. We show here that epithelial polarity and barrier function were directly affected upon WNT modulation, WNT activation inducing disruption of epithelial polarity, with decreased expression of PIGR/SC and of junctional proteins (*CDH1* and *TJP1*/ZO-1), whereas WNT inhibition improved both polarity and barrier function in COPD-derived ALI-HBEC. This study also shows that WNT/β-catenin activation increases the canonical TGF-β signalling – witnessed by increased TGF-β_1 production and SMAD2 phosphorylation – and induces EMT, whereas its inhibition decreased those signals. As EMT encompasses the loss of junctional proteins (occludin, E-cadherin) and impaired epithelial polarity, those features probably result from activation of an early EMT programming. Alternatively, they could less likely represent separate events of epithelial dysregulation that occur concomitantly. These observations are consistent with previous studies depicting a tight and complex crosstalk between WNT/β-catenin and TGF-β signalling pathways, which is required to promote EMT in cancer and tissue fibrosis [62]. Taken together, these data suggest that dedifferentiation and EMT in the COPD proximal AE also relate, at least partly, to canonical WNT activation and cooperation with TGF-β signalling.

Our study has limitations. First, one cannot exclude an effect of treatments, particularly inhaled corticosteroids in severe patients, on the findings. Mometasone furoate restored impaired WNT/β-catenin activity in a murine model of spinal cord injury [63], and dexamethasone increased canonical WNT components expression in 16HBE cells as well as in the (small) airway epithelium in mice [64]. However, *in vitro* studies in primary human bronchial and nasal epithelial cells in ALI culture showed dexamethasone-induced (0•1 μM) upregulation of E-cadherin and junctional (but not nuclear) β-catenin [65,66], rather suggestive of WNT/β-catenin inhibition by corticosteroids. In addition, correlation with exacerbation or chronic bronchitis phenotypes could not be assessed in this cohort of patients. Second, genetic approaches to activate or silence WNT signalling have not been used in this study to validate data obtained by using chemical inhibitors, a limitation mostly due to the difficulty of obtaining stable transfectants from primary bronchial cells [12]. Third, in addition to showing activation of the WNT/β-catenin *in situ* and *in vitro*, we explored its role in promoting the COPD epithelial phenotype *in vitro*, in conditions that are unlikely to recapitulate the chronic nature of the disease. Similarly, the potential contribution of squamous metaplasia or epithelial dysplasia was not evaluated. Finally, a conditional (or inducible) and targeted genetic model with gain- or loss-of-function mutations in β-catenin[67] within the adult mouse AE could be valuable to confirm the implications of our findings for *in vivo* lung homoeostasis and disease development, whereas such model remains to be established.

In conclusion, this study indicates that the WNT/β-catenin pathway is upregulated in the proximal AE from COPD patients, probably within progenitor basal cells, contributing to the abnormal airway epithelial phenotype in this disease. It also shows that the inhibition of this pathway restores epithelial homoeostasis in the cultured epithelium from severe COPD patients, not only for lineage differentiation but also for epithelial polarity, barrier function, and EMT. Finally, it provides further evidence of WNT crosstalk with canonical TGF-β activation, which in turn induces EMT. This evidence could thus represent a proof-of-concept study paving the way to therapeutic targeting of WNT/β-catenin or its downstream effectors in the COPD lung, providing it is selectively focussed on the lower airway (and not alveolar) epithelium. It also advocates for a better understanding of the implication of developmental pathways (and how they cooperate) in the adult lung signalling network.

Author contributions

FMC performed experiments, data analysis, co-supervised the experimental design and wrote the manuscript. SD designed the RNA-sequencing. JA performed the RNA-sequencing statistical analysis. BD helped with cell cultures. ML processed samples and helped with PCR and manuscript writing. CBC helped with β-catenin staining. YB performed the validation PCR and helped with WNT modulation experiments. JLG helped with RNA-sequencing design. CB helped with staining analysis. SEV and DH provided lung tissue samples. SG performed staining on ALI cultures and helped with the cell-type quantification. BB participated in the design of the RNA-sequencing panel. CP supervised the design of the study and the writing of the manuscript.

Funding

This work was supported by the Fondation Mont-Godinne, Belgium, grant to FC (N°FMG-2015-BC01, FMG-2016-BC01, and FMG-2017-BC01) by the Fonds National de Recherche Scientifique (FNRS),

Belgium, grant to FC (N°1.L505.18) and to CP (N°1.R016.16 and 1.R016.18), and by the Institute for Walloon Excellence in Lifesciences and Biotechnology (WELBIO CR-2012S-05). Funders were not involved in study design, data collection, data analysis, interpretation, or writing of the manuscript.

Declaration of Competing Interest

The authors have nothing to disclose.

Acknowledgements

The authors thank Drs. Lacroix, Rondelet, and Stanciu-Pop for providing surgical tissue, Mrs. Daumerie for technical advices, and Mrs. de Beukelaer and Fregimilicka for helping with the staining.

Supplementary materials

Supplementary material associated with this article can be found, in the online version, at doi:10.1016/j.ebiom.2020.103034.

References

[1] World Health Organization. Global health estimates 2016: estimated deaths by age, sex, and cause. 2016 https://www.who.int/healthinfo/global_burden_disease/estimates/en/. Accessed March 15, 2020.
[2] Salvi SS, Barnes PJ. Chronic obstructive pulmonary disease in non-smokers. Lancet 2009;374(9691):733–43.
[3] Vogelmeier CF, Criner GJ, Martinez FJ, et al. Global strategy for the diagnosis, management, and prevention of chronic obstructive lung disease 2017 report. Gold executive summary. Am J Respir Crit Care Med 2017;195(5):557–82.
[4] Saetta M. Airway inflammation in chronic obstructive pulmonary disease. Am J Respir Crit Care Med 1999;160(5 Pt 2):S17–20.
[5] Pini L, Pinelli V, Modina D, Bezzi M, Tiberio L, Tantucci C. Central airways remodeling in COPD patients. Int J Chron Obstruct Pulmon Dis 2014;9:927–32.
[6] Gohy S, Carlier FM, Fregimilicka C, et al. Altered generation of ciliated cells in chronic obstructive pulmonary disease. Sci Rep 2019;9(1):17963.
[7] Carlier F, Detry B, Sibille Y, Pilette C. COPD epithelial phenotype shows partial reversibility in long-term primary epithelial ALI-cultures. Eur Respir J 2018;52 (suppl 62).
[8] Aghapour M, Raee P, Moghaddam SJ, Hiemstra PS, Heijink IH. Airway epithelial barrier dysfunction in chronic obstructive pulmonary disease: role of cigarette smoke exposure. Am J Respir Cell Mol Biol 2018;58(2):157–69.
[9] Sohal SS. Chronic Obstructive pulmonary disease (COPD) and lung cancer: epithelial mesenchymal transition (EMT), the missing link? EBioMedicine 2015;2 (11):1578–9.
[10] Nusse R, Varmus HE. Many tumors induced by the mouse mammary tumor virus contain a provirus integrated in the same region of the host genome. Cell 1982;31(1):99–109.
[11] Gavin BJ, McMahon JA, McMahon AP. Expression of multiple novel Wnt-1/int-1-related genes during fetal and adult mouse development. Genes Dev 1990;4 (12B):2319–32.
[12] Baarsma HA, Konigshoff M. 'WNT-er is coming': WNT signalling in chronic lung diseases. Thorax 2017;72(8):746–59.
[13] Konigshoff M, Eickelberg O. WNT signaling in lung disease: a failure or a regeneration signal? Am J Respir Cell Mol Biol 2010;42(1):21–31.
[14] Angers S, Moon RT. Proximal events in Wnt signal transduction. Nat Rev Mol Cell Biol 2009;10(7):468–77.
[15] Nusse R, Clevers H. Wnt/beta-catenin signaling, disease, and emerging therapeutic modalities. Cell 2017;169(6):985–99.
[16] Metcalfe C, Mendoza-Topaz C, Mieszczanek J, Bienz M. Stability elements in the LRP6 cytoplasmic tail confer efficient signalling upon DIX-dependent polymerization. J Cell Sci 2010;123(Pt 9):1588–99.
[17] Eapen MS, Sharma P, Gaikwad AV, et al. Epithelial-mesenchymal transition is driven by transcriptional and post transcriptional modulations in COPD: implications for disease progression and new therapeutics. Int J Chron Obstruct Pulmon Dis 2019;14:1603–10.
[18] Boucherat O, Morissette MC, Provencher S, Bonnet S, Maltais F. Bridging lung development with chronic obstructive pulmonary disease. relevance of developmental pathways in chronic obstructive pulmonary disease pathogenesis. Am J Respir Crit Care Med 2016;193(4):362–75.
[19] Baarsma HA, Skronska-Wasek W, Mutze K, et al. Noncanonical WNT-5A signaling impairs endogenous lung repair in COPD. J Exp Med 2017;214(1):143–63.
[20] Wu X, van Dijk EM, Ng-Blichfeldt JP, et al. Mesenchymal WNT-5A/5B signaling represses lung alveolar epithelial progenitors. Cells 2019;8(10).
[21] Skronska-Wasek W, Mutze K, Baarsma HA, et al. Reduced frizzled receptor 4 expression prevents WNT/beta-catenin-driven alveolar lung repair in chronic obstructive pulmonary disease. Am J Respir Crit Care Med 2017;196(2):172–85.
[22] Kneidinger N, Yildirim AO, Callegari J, et al. Activation of the WNT/beta-catenin pathway attenuates experimental emphysema. Am J Respir Crit Care Med 2011;183(6):723–33.
[23] Uhl FE, Vierkotten S, Wagner DE, et al. Preclinical validation and imaging of Wnt-induced repair in human 3D lung tissue cultures. Eur Respir J 2015;46(4):1150–66.
[24] Cho MH, McDonald ML, Zhou X, et al. Risk loci for chronic obstructive pulmonary disease: a genome-wide association study and meta-analysis. Lancet Respir Med 2014;2(3):214–25.
[25] Jiang Z, Lao T, Qiu W, et al. A chronic obstructive pulmonary disease susceptibility gene, FAM13A, regulates protein stability of beta-catenin. Am J Respir Crit Care Med 2016;194(2):185–97.
[26] Durham AL, McLaren A, Hayes BP, et al. Regulation of Wnt4 in chronic obstructive pulmonary disease. FASEB J 2013;27(6):2367–81.
[27] Heijink IH, de Bruin HG, van den Berge M, et al. Role of aberrant WNT signalling in the airway epithelial response to cigarette smoke in chronic obstructive pulmonary disease. Thorax 2013;68(8):709–16.
[28] Heijink IH, de Bruin HG, Dennebos R, et al. Cigarette smoke-induced epithelial expression of WNT-5B: implications for COPD. Eur Respir J 2016;48 (2):504–15.
[29] Zou W, Zou Y, Zhao Z, Li B, Ran P. Nicotine-induced epithelial-mesenchymal transition via Wnt/beta-catenin signaling in human airway epithelial cells. Am J Physiol Lung Cell Mol Physiol 2013;304(4):L199–209.
[30] Spanjer AI, Menzen MH, Dijkstra AE, et al. A pro-inflammatory role for the Frizzled-8 receptor in chronic bronchitis. Thorax 2016;71(4):312–22.
[31] Malleske DT, Hayes Jr. D, Lallier SW, Hill CL, Reynolds SD. Regulation of human airway epithelial tissue stem cell differentiation by beta-catenin, P300, and CBP. Stem Cells 2018.
[32] Wang R, Ahmed J, Wang G, et al. Down-regulation of the canonical Wnt beta-catenin pathway in the airway epithelium of healthy smokers and smokers with COPD. PLoS ONE 2011;6(4):e14793.
[33] Guo L, Wang T, Wu Y, et al. WNT/beta-catenin signaling regulates cigarette smoke-induced airway inflammation via the PPARdelta/p38 pathway. Lab Invest 2016;96:218–29.
[34] Lamouille S, Xu J, Derynck R. Molecular mechanisms of epithelial-mesenchymal transition. Nat Rev Mol Cell Biol 2014;15(3):178–96.
[35] Milara J, Peiro T, Serrano A, Cortijo J. Epithelial to mesenchymal transition is increased in patients with COPD and induced by cigarette smoke. Thorax 2013;68 (5):410–20.
[36] Sohal SS, Reid D, Soltani A, et al. Reticular basement membrane fragmentation and potential epithelial mesenchymal transition is exaggerated in the airways of smokers with chronic obstructive pulmonary disease. Respirology 2010;15 (6):930–8.
[37] Sohal SS, Reid D, Soltani A, et al. Evaluation of epithelial mesenchymal transition in patients with chronic obstructive pulmonary disease. Respir Res 2011;12:130.
[38] Bartis D, Mise N, Mahida RY, Eickelberg O, Thickett DR. Epithelial-mesenchymal transition in lung development and disease: does it exist and is it important? Thorax 2014;69(8):760–5.
[39] Jolly MK, Ward C, Eapen MS, et al. Epithelial-mesenchymal transition, a spectrum of states: role in lung development, homeostasis, and disease. Dev Dyn 2018;247 (3):346–58.
[40] Gohy ST, Hupin C, Fregimilicka C, et al. Imprinting of the COPD airway epithelium for dedifferentiation and mesenchymal transition. Eur Respir J 2015;45(5):1258–72.
[41] Baarsma HA, Spanjer AI, Haitsma G, et al. Activation of WNT/beta-catenin signaling in pulmonary fibroblasts by TGF-beta(1) is increased in chronic obstructive pulmonary disease. PLoS ONE 2011;6(9):e25450.
[42] Benjamini Y, Hochberg Y. Controlling the false discovery rate: a practical and powerful approach to multiple testing. J R Statis Soc 1995;57(1):289–300.
[43] Bustin SA, Benes V, Garson J, et al. The need for transparency and good practices in the qPCR literature. Nat Methods 2013;10(11):1063–7.
[44] Pilette C, Ouadrhiri Y, Dimanche F, Vaerman JP, Sibille Y. Secretory component is cleaved by neutrophil serine proteinases but its epithelial production is increased by neutrophils through NF-kappa B- and p38 mitogen-activated protein kinase-dependent mechanisms. Am J Respir Cell Mol Biol 2003;28(4):485–98.
[45] Pilette C, Godding V, Kiss R, et al. Reduced epithelial expression of secretory component in small airways correlates with airflow obstruction in chronic obstructive pulmonary disease. Am J Respir Crit Care Med 2001;163(1):185–94.
[46] Simoes A, Chen Z, Zhao Y, et al. Laser capture microdissection of epithelium from a wound healing model for MicroRNA analysis. Methods Mol Biol 2018;1733: 225–37.
[47] Gohy ST, Detry BR, Lecocq M, et al. Polymeric immunoglobulin receptor down-regulation in chronic obstructive pulmonary disease. Persistence in the cultured epithelium and role of transforming growth factor-beta. Am J Respir Crit Care Med 2014;190(5):509–21.
[48] Mahmood MQ, Walters EH, Shukla SD, et al. beta-catenin, Twist and Snail: transcriptional regulation of EMT in smokers and COPD, and relation to airflow obstruction. Sci Rep 2017;7(1):10832.
[49] Clevers H. Wnt/beta-catenin signaling in development and disease. Cell 2006;127 (3):469–80.
[50] Schmid A, Sailland J, Novak L, Baumlin N, Fregien N, Salathe M. Modulation of Wnt signaling is essential for the differentiation of ciliated epithelial cells in human airways. FEBS Lett 2017;591(21):3493–506.
[51] Brechbuhl HM, Ghosh M, Smith MK, et al. beta-catenin dosage is a critical determinant of tracheal basal cell fate determination. Am J Pathol 2011;179(1):367–79.

[52] Domyan ET, Sun X. Patterning and plasticity in development of the respiratory lineage. Dev Dyn 2011;240(3):477–85.
[53] Konigshoff M, Kneidinger N, Eickelberg O. TGF-beta signaling in COPD: deciphering genetic and cellular susceptibilities for future therapeutic regimen. Swiss Med Wkly 2009;139(39–40):554–63.
[54] Boucherat O, Chakir J, Jeannotte L. The loss of Hoxa5 function promotes Notch-dependent goblet cell metaplasia in lung airways. Biol Open 2012;1(7):677–91.
[55] Li S, Hu X, Wang Z, Wu M, Zhang J. Different profiles of notch signaling in cigarette smoke-induced pulmonary emphysema and bleomycin-induced pulmonary fibrosis. Inflamm Res 2015;64(5):363–71.
[56] Tilley AE, Harvey BG, Heguy A, et al. Down-regulation of the notch pathway in human airway epithelium in association with smoking and chronic obstructive pulmonary disease. Am J Respir Crit Care Med 2009;179(6):457–66.
[57] Whitsett JA, Kalinichenko VV. Notch and basal cells take center stage during airway epithelial regeneration. Cell Stem Cell 2011;8(6):597–8.
[58] Kugler MC, Joyner AL, Loomis CA, Munger JS. Sonic hedgehog signaling in the lung. From development to disease. Am J Respir Cell Mol Biol 2015;52(1):1–13.
[59] Ruiz Garcia S, Deprez M, Lebrigand K, et al. Novel dynamics of human mucociliary differentiation revealed by single-cell RNA sequencing of nasal epithelial cultures. Development 2019;146(20).
[60] Mucenski ML, Nation JM, Thitoff AR, et al. Beta-catenin regulates differentiation of respiratory epithelial cells *in vivo*. Am J Physiol Lung Cell Mol Physiol 2005;289(6):L971–9.
[61] Heijink IH, Postma DS, Noordhoek JA, Broekema M, Kapus A. House dust mite-promoted epithelial-to-mesenchymal transition in human bronchial epithelium. Am J Respir Cell Mol Biol 2010;42(1):69–79.
[62] Vallee A, Lecarpentier Y, Guillevin R, Vallee JN. Interactions between TGF-beta1, canonical WNT/beta-catenin pathway and PPAR gamma in radiation-induced fibrosis. Oncotarget 2017;8(52):90579–604.
[63] Libro R, Giacoppo S, Bramanti P, Mazzon E. Is the Wnt/beta-catenin pathway involved in the anti-inflammatory activity of glucocorticoids in spinal cord injury? Neuroreport 2016;27(14):1086–94.
[64] Yu Z, Jiang Y, Sun C. Glucocorticoids inhibits the repair of airway epithelial cells via the activation of wnt pathway. Respir Physiol Neurobiol 2020;271:103283.
[65] Carayol N, Vachier I, Campbell A, et al. Regulation of E-cadherin expression by dexamethasone and tumour necrosis factor-alpha in nasal epithelium. Eur Respir J 2002;20(6):1430–6.
[66] Carayol N, Campbell A, Vachier I, et al. Modulation of cadherin and catenins expression by tumor necrosis factor-alpha and dexamethasone in human bronchial epithelial cells. Am J Respir Cell Mol Biol 2002;26(3):341–7.
[67] Harris-Johnson KS, Domyan ET, Vezina CM, Sun X. beta-Catenin promotes respiratory progenitor identity in mouse foregut. Proc Natl Acad Sci U S A 2009;106(38):16287–92.